

# Thermal Stability and Decomposition Pathways in Volatile Molybdenum(VI) Bis-Imides

Michael A. Land,<sup>\*[a]</sup> Goran Bačić,<sup>[a]</sup> Katherine N. Robertson,<sup>[b]</sup> and Seán T. Barry<sup>[a]</sup>

[a] M. A. Land, Dr. G. Bačić, Prof. S. T. Barry  
Department of Chemistry, Carleton University  
1125 Colonel By Drive, Ottawa, Ontario, K1S 5B6 Canada  
E-mail: Michael.land@carleton.ca

[b] Dr. K. N. Robertson  
Department of Chemistry, Saint Mary's University  
923 Robie Street, Halifax, Nova Scotia, B3H 3C3 Canada

Supporting information for this article is given *via* a link at the end of the document.

**Abstract:** The vapor deposition of many molybdenum-containing films relies on the delivery of volatile compounds with the general *bis(tert-butylimido)molybdenum(VI)* framework, both in atomic layer deposition and chemical vapor deposition. We have prepared a series of (tBuN)<sub>2</sub>MoCl<sub>2</sub> adducts using neutral *N,N'*-chelates and investigated their volatility, thermal stability, and decomposition pathways. Volatility has been determined by thermogravimetric analysis, with the 1,4-di-*tert*-butyl-1,3-diazabutadiene adduct (**5**) found to be the most volatile (1 Torr of vapor pressure at 135 °C). Thermal stability was measured primarily using differential scanning calorimetry, and the 1,10-phenanthroline adduct (**4**) was found to be the most stable, with an onset of decomposition of 303 °C. We have also investigated molybdenum compounds with other alkyl-substituted imido groups: these compounds all follow a similar decomposition pathway,  $\gamma$ -H activation, with varying reaction barriers. The *tert*-pentyl, 1-adamantyl, and a cyclic imido (from 2,5-dimethylhexane-2,5-diamine) were systematically studied to probe the kinetics of this pathway. All of these compounds have been fully characterized, including *via* single-crystal X-ray diffraction, and a total of 19 unique structures are reported.

## Introduction

Molybdenum-containing films have a wide array of applications including: microelectronic manufacturing,<sup>[1]</sup> high-surface area heterogeneous catalysis,<sup>[2]</sup> gas-sensing,<sup>[3]</sup> optical materials,<sup>[4]</sup> and lubricants.<sup>[5]</sup> Chemical vapor deposition (CVD) and atomic layer deposition (ALD) are two popular methods to prepare Mo-containing films; CVD is a continuous technique while ALD is a stepwise layer-by-layer method. Both produce uniform and high-quality thin films, which ALD does with sub-nanometer thickness control.<sup>[6,7]</sup> Both techniques rely on chemical precursors that can be delivered in the vapor phase to the substrate where they subsequently undergo gas-surface reactions to grow thin films.

The most important criteria in the design of potential precursors are thermal stability, volatility, and surface reactivity.<sup>[8]</sup> Thermal stability is particularly important in ALD because the formation of stable self-limiting monolayers is the main difference between ALD and CVD.<sup>[6,7]</sup> For example, compounds must have adequate thermal stability in a precursor container during deposition to ensure that: 1) the payload atom is delivered into the reaction chamber without decomposition into a non-volatile material, 2) consistent gas phase precursor concentrations are

maintained throughout a deposition, and 3) the identity of the gas-phase species is known to help interrogate reaction mechanisms in the gas phase and at the surface. A review of the experimental and theoretical approaches that have been used to evaluate and predict the thermal stability of precursor molecules has been previously published.<sup>[9]</sup>

Predicting the volatility of new molecules *a priori* is difficult, so deriving frameworks from compounds that have already been successfully utilized can provide a useful starting point for designing new precursors. The general *bis(tert-butylimido)molybdenum(VI)* framework can be easily modified by changing either the neutral ligands (**I**, Chart 1) or the anionic ligands (**II**),<sup>[10]</sup> and it has been incorporated into several molybdenum precursors. For example, *bis(tert-butylimido)-bis(dimethylamido)molybdenum(VI)* (**A**) has been used as a precursor for the ALD of MoN<sub>x</sub>,<sup>[11,12]</sup> MoO<sub>3</sub>,<sup>[13,14]</sup> MoS<sub>2</sub>,<sup>[15–17]</sup> MoC<sub>x</sub>N<sub>y</sub>,<sup>[18,19]</sup> TiMo<sub>x</sub>N<sub>y</sub>,<sup>[20]</sup> and Al:MoS<sub>2</sub>.<sup>[21]</sup> *N,N'*-chelating ligands have also been used to prepare volatile *bis(tert-butylimido)-molybdenum(VI)* compounds, such as amidinates (**B**),<sup>[22]</sup> pyrazolates (**C**),<sup>[10]</sup> guanidinates (**D**),<sup>[23]</sup> and diazabutadienyls (**E**).<sup>[24]</sup> However, only the amidinate **B** has been used for ALD to prepare MoO<sub>3</sub> films with O<sub>3</sub>.<sup>[3]</sup> It has also been used by CVD for the deposition of MoS<sub>2</sub><sup>[25]</sup> and MoN<sub>x</sub>.<sup>[22,26]</sup> The pyrazolate **C** and the guanidinates **D** have been used as single-source precursors for the CVD of Mo<sub>2</sub>N<sup>[27]</sup> and MoC<sub>x</sub>N<sub>y</sub>,<sup>[28]</sup> respectively, whereas MoS<sub>2</sub> films have been prepared by CVD with the diazabutadienyl **E** and S<sub>8</sub>.<sup>[24]</sup> The thiolate compound (**F**) has been used for the ALD

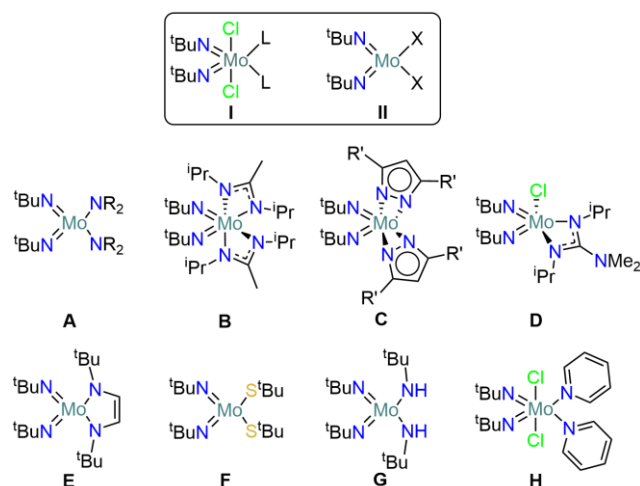


**Chart 1.** General *bis(tert-butylimido)molybdenum(VI)* frameworks, and known ALD and CVD precursors that incorporate them. L = neutral ligand, X = anionic ligand, R = Me or Et, R' = tBu or Ph.

of Mo<sub>2</sub>N films, with H<sub>2</sub> plasma,<sup>[29]</sup> and for the CVD of nitrogen-doped MoS<sub>2</sub>.<sup>[30]</sup> Finally, both the amido (**G**) and the chloro (**H**) compounds have been used for the CVD of MoC<sub>x</sub>N<sub>y</sub>.<sup>[31,32]</sup>

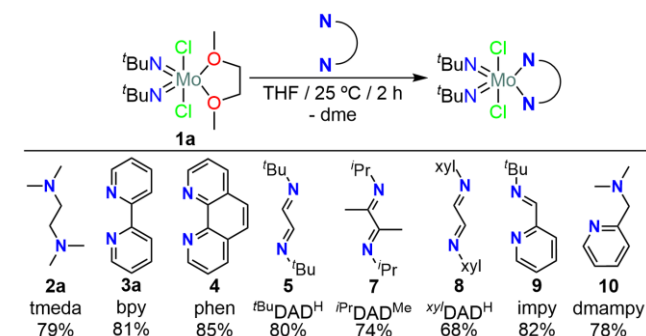
We have previously explored the volatility and thermal stability of the dichloro-substituted (<sup>t</sup>BuN)<sub>2</sub>MoCl<sub>2</sub>-L (L = neutral ligand) framework (**I**, Chart 1) and studied the effect of amines, phosphines, ethers and *N*-heterocyclic carbenes when used as the neutral ligand.<sup>[33]</sup> Some of these coordinating ligands increased the volatility of this framework but were found to dissociate from the metal complex during evaporation. This so-called “ligand-assisted volatilization” is a convenient method to improve the volatility of a compound. However, it is detrimental for CVD and ALD precursors as it changes the concentration and the composition of the vapor phase over time, in turn, affecting the deposition kinetics and complicating the deposition mechanism. We also found that neutral *N,N'*-chelate ligands did not dissociate from the metal complex upon heating and evaporation.<sup>[33]</sup> Thus, in this work we have prepared a series of *bis*(alkylimido)-dichloromolybdenum(VI) complexes and investigated how different neutral *N,N'*-chelating ligands (Scheme 1) as well as different alkylimido groups affect volatility and thermal stability.

## Results and Discussion

### Synthesis and Characterization

The starting material (<sup>t</sup>BuN)<sub>2</sub>MoCl<sub>2</sub>-dme (**1a**) was conveniently prepared following known methods from Na<sub>2</sub>MoO<sub>4</sub>.<sup>[34,35]</sup> We then directly treated **1a** with *N,N,N',N'*-tetramethylethylenediamine (tmeda) or 2,2'-bipyridine (bpy) to prepare (<sup>t</sup>BuN)<sub>2</sub>MoCl<sub>2</sub>-tmeda (**2a**) and (<sup>t</sup>BuN)<sub>2</sub>MoCl<sub>2</sub>-bpy (**3a**), respectively, following our previously reported method (Scheme 1).<sup>[33]</sup> In our initial synthesis of **2a**, we found small amounts of an unidentified non-volatile impurity (despite obtaining adequate combustion analysis data) which was easily removed by recrystallizing **2a** from a toluene/pentane solution. Considering this, all new compounds reported herein were purified by crystallization or sublimation as a precaution and updated thermal properties of the pure materials are reported.

From our previous study it was apparent that the bpy adduct **3a** provided superior thermal stability and we were interested to see if other heteroaromatic ligands would do the same. Specifically, 1,10-phenanthroline was chosen because of its accessibility compared to substituted bipyridines. Thus, a hexane solution of **1a** was treated with 1,10-phenanthroline (phen) which resulted in the immediate precipitation of (<sup>t</sup>BuN)<sub>2</sub>MoCl<sub>2</sub>-phen (**4**)



**Scheme 1.** Synthesis of the (<sup>t</sup>BuN)<sub>2</sub>MoCl<sub>2</sub> adducts discussed herein. The general framework is shown in the reaction scheme and the specific ligands are shown below (with their adduct numbering, abbreviations, and yields). <sup>t</sup>Bu = *tert*-butyl, <sup>i</sup>Pr = isopropyl, *xy*l = 2,6-dimethylphenyl.

as a yellow powder. Initially the product was found to be contaminated with **1a**, even if a two-fold excess of phen was used and the mixture was stirred overnight. Switching the solvent from hexane to THF allowed complete exchange of the ligand and after optimization **4** was isolated in high yield.

Both bpy and 1,4-diazabutadienes (DAD) are 1,2-diimines, so we also investigated them here, in hopes that they would confer additional volatility to the products we prepared. Arguably the most commonly explored neutral *N,N'*-chelate in organometallic chemistry,<sup>[36]</sup> DAD can be easily tailored to probe various electronic and steric effects. Compounds with DAD ligands are also redox active, and the doubly-reduced 1,4-di-*tert*-butyl-1,3-diazabutadienyl ligand had previously been used to prepare the volatile *bis*(*tert*-butylimido)-molybdenum(VI) compound (**E**).<sup>[24]</sup> Direct treatment of **1a** with 1,4-di-*tert*-butyl-1,3-diazabutadiene (<sup>t</sup>BuDAD<sup>H</sup>) in THF gave (<sup>t</sup>BuN)<sub>2</sub>MoCl<sub>2</sub>·(<sup>t</sup>BuDAD<sup>H</sup>) (**5**) in good yield.

The <sup>t</sup>BuDAD<sup>H</sup> adduct **5** undergoes either partial hydrolysis or oxidation upon air exposure, and a single crystal of (<sup>t</sup>BuN)MoOCl<sub>2</sub>·(<sup>t</sup>BuDAD<sup>H</sup>) (**6**) was isolated serendipitously (*vide infra*). Compound **6** contains a strong Mo=O bond which is generally to be avoided in precursor ligand environments; it could lead to oxygen incorporation in a deposited film. However, for completeness we chose to rationally prepare and thermally characterize this compound since this feature would not be detrimental in the preparation of oxygen-containing target films (*i.e.* MoO<sub>3</sub> or MoO<sub>x</sub>N<sub>y</sub>). Compound **6** was made by treating (<sup>t</sup>BuN)MoOCl<sub>2</sub>-dme with <sup>t</sup>BuDAD<sup>H</sup> (Scheme 2); the <sup>1</sup>H NMR data has been previously reported.<sup>[37]</sup> The <sup>1</sup>H and <sup>13</sup>C NMR spectra of **6** were straightforward and showed the expected asymmetry arising from the oxo moiety. To ensure that the bulk material of **6** was not a solid mixture of **5** and MoO<sub>2</sub>Cl<sub>2</sub>·(<sup>t</sup>BuDAD<sup>H</sup>),<sup>[38]</sup> authentic samples of both compounds were combined in C<sub>6</sub>D<sub>6</sub> and the <sup>1</sup>H NMR spectrum showed them to be two discrete species (Figure S144).

Due to the ready accessibility of substituted diazabutadienes, and because they can generate volatile frameworks, we further investigated their use.<sup>[24,39,40]</sup> Treatment of **1a** with 1,4-di-isopropyl-2,3-dimethyl-1,3-diazabutadiene (<sup>i</sup>PrDAD<sup>Me</sup>) resulted in the isolation of (<sup>t</sup>BuN)<sub>2</sub>MoCl<sub>2</sub>·(<sup>i</sup>PrDAD<sup>Me</sup>) (**7**), which is a structural isomer of **5**. NMR spectroscopy and X-ray diffraction confirmed that the ligand coordinated to the molybdenum center as a neutral *N,N'*-chelate (*vide infra*), and not as an anionic *N,C*-chelate as has been found for other 2,3-dimethyl-1,3-diazabutadienes.<sup>[41]</sup> Likewise, treatment of **1a** with 1,4-*bis*(2,6-dimethylphenyl)-1,3-diazabutadiene (<sup>xy</sup>lDAD<sup>H</sup>) resulted in the isolation of (<sup>t</sup>BuN)<sub>2</sub>MoCl<sub>2</sub>·(<sup>xy</sup>lDAD<sup>H</sup>) (**8**) in moderate yield.

Following the preparation of the compounds incorporating different *N,N'*-chelating ligands we were interested in preparing hybrid ligands to see if we could tailor their thermal properties to our needs. For example, bpy provides excellent thermal stability, whereas use of <sup>t</sup>BuDAD<sup>H</sup> is expected to result in a very volatile compound. Following this rationale, we chose a ligand that is



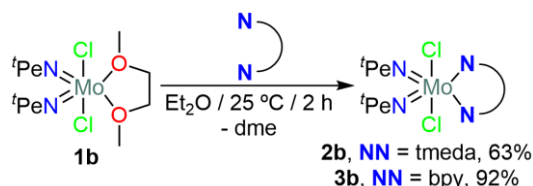
**Scheme 2.** Synthesis of (<sup>t</sup>BuN)MoOCl<sub>2</sub>·(<sup>t</sup>BuDAD<sup>H</sup>) **6**.

structural combination of  ${}^t\text{BuDAD}^{\text{H}}$  and bpy; *tert*-butyl(pyridine-2-yl-methyleneamine) (impy). Treatment of impy with the dme adduct **1a** in THF resulted in the isolation of  $({}^t\text{BuN})_2\text{MoCl}_2\text{-impy}$  (**9**) as a yellow powder in good yield. The  ${}^1\text{H}$  NMR spectrum of **9** showed the *tert*-butylimido moieties to be magnetically equivalent, giving rise to one singlet. However,  ${}^{13}\text{C}$  NMR spectroscopy revealed two chemical environments for the same moieties, confirming ligand asymmetry. We also prepared a compound using a hybrid ligand with one pyridine and one amine group in a chelate, 2-(*N,N*-dimethylamino)methylpyridine (dmampy);  $({}^t\text{BuN})_2\text{MoCl}_2\text{-dmampy}$  (**10**) was isolated in moderate yield. This unusual ligand has only been used in a few structures that have been deposited to the Cambridge Structural Database.<sup>[42–44]</sup> As anticipated both the  ${}^1\text{H}$  and  ${}^{13}\text{C}$  NMR spectra of **10** revealed inequivalent *tert*-butylimido moieties. Finally, we tried to prepare a molybdenum compound using a hybrid ligand that combined tmeda and  ${}^t\text{BuDAD}^{\text{H}}$ . However, treatment of **1a** with the  $\alpha$ -aminoaldimine, 1-(*tert*-butylimino)-*N,N*,2-trimethylpropan-2-amine (imtmpa),<sup>[45]</sup> consistently resulted in the isolation of the ionic salt, [imtmpaH][ $({}^t\text{BuN})_2\text{MoCl}_3$ ]. This salt likely forms from decomposition of an unidentified intermediate, a process which is further discussed in the SI. Salts containing the  $[(\text{RN})_2\text{MoCl}_3]$  anion are rare having only been reported twice before.<sup>[33,46]</sup>

With this series of  $({}^t\text{BuN})_2\text{MoCl}_2$  adducts in hand, we then began exploring the effect of changing the imido substituents. This was done to investigate how this portion of the molecule alters volatility, and more importantly thermal stability. We only investigated imido groups bound to a quaternary carbon atom, to allow exploration of the similar  $\gamma$ -elimination mechanism that these compounds would have to undergo. We did not prepare compounds of the type  $(\text{RN})_2\text{MoCl}_2$  where the R group contains  $\beta$ -hydrogens, which would let a competing elimination reaction occur.<sup>[47]</sup> Therefore, we chose to investigate complexes containing *tert*-pentyl (*i.e.*, *tert*-amyl) imido groups. Interestingly, there is only one example of a Mo(VI) adduct containing a ligand of this type in the literature.<sup>[48]</sup>

Treatment of the dme adduct **1b** with tmeda in pentane resulted in the formation of  $({}^t\text{PeN})_2\text{MoCl}_2\text{-tmeda}$  (**2b**) as a waxy orange solid. The spectroscopically pure product was obtained after a combination of lyophilization and crystallization (Scheme 3). Following a similar method, the analogous bpy adduct,  $({}^t\text{PeN})_2\text{MoCl}_2\text{-bpy}$  (**3b**) was also isolated in high yield. Attempts to prepare a  ${}^t\text{BuDAD}^{\text{H}}$  adduct from **1b** only led to the isolation of starting materials. This lack of reactivity is likely due to the steric bulk of the imido groups congesting the inner coordination sphere, preventing the coordination of  ${}^t\text{BuDAD}^{\text{H}}$ .

The primary decomposition pathway of the  $({}^t\text{BuN})_2\text{MoCl}_2$  compounds occurs through the  $\gamma$ -H activation of the *tert*-butyl groups and is rapid due to the formation of the very volatile by-product (isobutylene).<sup>[33]</sup> The *tert*-pentyl adducts **2b** and **3b** would likely have analogous decomposition pathways. Therefore, we attempted to block this primary decomposition pathway by tethering the two imido groups together, to try and prevent this single-step decomposition. To achieve this, we prepared the



**Scheme 3.** Synthesis of the  $({}^t\text{PeN})_2\text{MoCl}_2$  adducts.  ${}^t\text{Pe}$  = *tert*-pentyl.



**Scheme 4.** Synthesis of the  $(\text{NCMe}_2(\text{CH}_2)_2\text{CMe}_2\text{N})\text{MoCl}_2$  adducts.

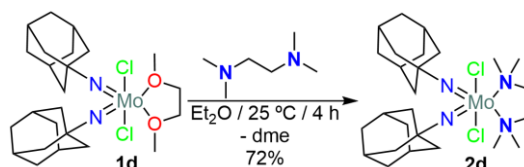
uncommon imido molybdenum(VI) framework,  $(\text{NCMe}_2(\text{CH}_2)_2\text{CMe}_2\text{N})\text{MoCl}_2\text{-dme}$  (**1c**), *via* treatment of 2,5-dimethylhexane-2,5-diamine with sodium molybdate, chlorotrimethylsilane, and triethylamine in dme.<sup>[49]</sup> Treatment of **1c** with tmeda in diethyl ether resulted in the formation of  $(\text{NCMe}_2(\text{CH}_2)_2\text{CMe}_2\text{N})\text{MoCl}_2\text{-tmeda}$  (**2c**) in moderate yield (Scheme 4). Compound **2c** was then treated with bpy and  $(\text{NCMe}_2(\text{CH}_2)_2\text{CMe}_2\text{N})\text{MoCl}_2\text{-bpy}$  (**3c**) was isolated in good yield, showcasing the labile nature of the *N,N'*-chelating ligands. Characterization of **2c** using  ${}^1\text{H}$  NMR spectroscopy proved challenging. At room temperature, the  $(\text{CH}_2)_2$  protons on the backbone of the metallocycle imido ligand were hidden in the baseline due to their rapid exchange on the NMR time scale. However, when the spectrum was recollected at  $-20\text{ }^\circ\text{C}$ , signals for these protons appeared as two discrete doublets. The analogous protons in the  ${}^1\text{H}$  NMR spectrum of **3c** were observed at room temperature, appearing as a very broad singlet, also due to the coalescence of these two chemical environments. Interpretation of the  ${}^{13}\text{C}$  NMR spectrum of both **2c** and **3c** was straightforward, however, the  $\text{CMe}_2$  signal of the imido ligand was slightly broadened at room temperature. Finally, the solid-state structures of **2c** and **3c** were confirmed using X-ray crystallography, revealing spirocyclic structures (*vide infra*).

Finally, using  $(\text{AdN})_2\text{MoCl}_2\text{-dme}$  (**1d** (Ad = 1-adamantyl))<sup>[50]</sup> we prepared the tmeda adduct,  $(\text{AdN})_2\text{MoCl}_2\text{-tmeda}$  (**2d**) (Scheme 5). The adamantyl adduct was of interest for its quaternary carbon atom and because adamantyl groups are typically thermally robust. This stability is attributed to the fact that bridgehead alkenes are rare and often unstable,<sup>[51]</sup> according to Bredt's rule,<sup>[52]</sup> hindering low-temperature  $\gamma$ -H activation.

### X-ray Crystallography

The solid-state structures for all of the compounds described herein were determined using single-crystal X-ray diffraction. Additionally, we have included the crystal structures of the starting materials  $\text{MoO}_2\text{Cl}_2\text{-dme}$  and *bis-N,N'*-(2-chloroacetyl)-2,5-dimethylhexane-2,5-diamine, as well as those of [imtmpaH][ $({}^t\text{BuN})_2\text{MoCl}_3$ ] and  $({}^t\text{BuN})_2\text{MoCl}_2\text{-}({}^t\text{PeDAD}^{\text{H}})$  in the SI. The structures of the tmeda adduct **2a** and the bpy adduct **3a** have been reported previously.<sup>[33]</sup> The literature structure of **3a** contains benzene as a solvent of crystallization but here we report the structure both with (toluene, see SI) and without solvent. A summary of selected bond lengths and angles is shown in Table 1 and additional crystallographic parameters and images can be found in the supporting information.

The results from the single crystal X-ray structural studies of the tmeda adducts **2b-d** are shown in Figure 1. In all structures the molybdenum centers are octahedral with a *trans* disposition



**Scheme 5.** Synthesis of  $(\text{AdN})\text{MoCl}_2\text{-tmeda}$  (**2d**). Ad = 1-adamantyl.

**Table 1.** Selected bond lengths and angles.<sup>[a,b]</sup>

Compound	Mo–N(1/2) / Å	Mo–N(3/4) / Å	Mo–N(3/4)–C / °	Cl–Mo–Cl / °
<b>2a</b> <sup>[33]</sup>	2.525(7) 2.556(7)	1.7319(13) 1.7416(13)	167.54(12) 159.62(11)	165.77(2)
<b>2b</b> <sup>[c]</sup>	2.512(4) 2.529(3)	1.734(3) 1.736(3)	163.4(3) 162.8(3)	164.91(4)
<b>2c</b>	2.508(6) 2.532(7)	1.735[13] 1.736[8]	145.0[18] 147.7[6]	165.29(3)
<b>2d</b>	2.499(2) 2.554(2)	1.733(2) 1.740(2)	170.5(2) 157.5(2)	164.91(3)
<b>3a</b>	2.3732(6) 2.3761(6)	1.7425(6) 1.7466(6)	165.20(6) 162.86(6)	159.240(6)
<b>3b</b>	2.3671(17) 2.3952(17)	1.7395(18) 1.7469(18)	164[3] 166.04(17)	158.36(2)
<b>3c</b>	2.3677(11) 2.3916(12)	1.74[2] 1.74[3]	148.6[8] 149[4]	161.388(13)
<b>4</b>	2.375(6) 2.389(6)	1.734(7) 1.742(7)	168[5] 161.0(6)	159.61(7)
<b>5</b>	2.4972(5) 2.5210(5)	1.7455(5) 1.7461(5)	158.30(4) 162.83(4)	155.432(5)
<b>6</b> <sup>[c]</sup>	2.4082(10) 2.4710(11)	1.7305(10) -	159.09(9) -	156.963(12)
<b>7</b> <sup>[c]</sup>	2.3770(12) 2.4353(12)	1.7384(12) 1.7460(12)	163.96(12) 158[4]	158[2]
<b>8</b>	2.4646(9) 2.5252(9)	1.7354(9) 1.7387(10)	169.04(9) 164.20(8)	161.094(11)
<b>9</b>	2.399[4] 2.489[9]	1.731[15] 1.735[12]	161[2] 172[9]	160[2]
<b>10</b>	2.3669(13) 2.5261(14)	1.7366(14) 1.7401(14)	162.90(13) 164.87(15)	163.875(16)

[a] Uncertainties in curved brackets are the calculated uncertainty of one bond measurement; values in square brackets are the standard deviation from the mean of two measurements arising from disorder in the molecule.

[b] Bond lengths are always listed with the shorter bond first; the angles match the bond length order.

[c] If a structure (**2b**, **6**, or **7**) contained 2 molecules in the asymmetric unit, the parameters for molecule 1 are given.

of the chlorides. In all cases, the Mo–N(chelate) lengths are similar, suggesting that the binding of tmeda is not affected by the steric bulk of the imido moieties. Additionally, because the tmeda ligand appears to bind in the same manner in all examples, the Mo=N(imido) bond lengths are also similar (Table 1). However, between the four tmeda adducts there are noticeable differences in the imido bond angles. For example, the bond angles in **2a** and **2b** are both close to linear, due to their similar steric encumbrances. However, the analogous bond angles in **2c** are significantly bent due to metalocycle formation. Finally, the bond angles of the two imidos in **2d** are inequivalent with a 13° difference between them, likely a result of the space required by the sterically demanding adamantyl groups.

X-ray crystal structures of the 2,2-bipyridine adduct **3a** and the 1,10-phenanthroline adduct **4** are shown in Figure 2. The metal-nitrogen bond lengths of the chelates in both structures are

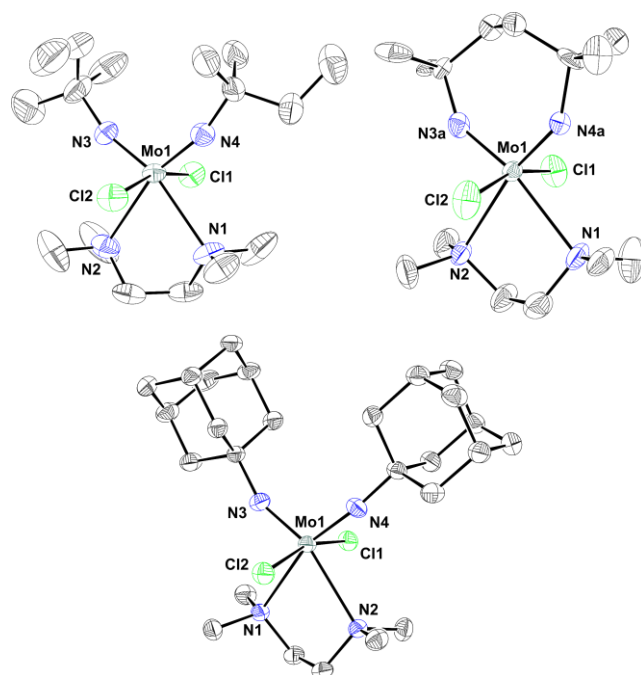


**Figure 1.** Solid-state structure of (*t*PeN)<sub>2</sub>MoCl<sub>2</sub>-tmeda **2b** (top left), (NCMe<sub>2</sub>(CH<sub>2</sub>)<sub>2</sub>CMe<sub>2</sub>N)MoCl<sub>2</sub>-tmeda **2c** (top right), and (AdN)<sub>2</sub>MoCl<sub>2</sub>-tmeda **2d** (bottom). Thermal ellipsoids are drawn at the 50% probability level. Hydrogen atoms have been omitted for visual clarity. There are two molecules in the asymmetric unit of **2b**, however, only molecule 1 is shown for visual clarity. Most of the molecule in **2c** is disordered over two positions however, only part A of the disorder is shown for visual clarity.

statistically equivalent, suggesting comparable  $\sigma$ -donation effects and steric profiles. The Mo–N4 imido bond length in **4** is short compared to the Mo–N3 bond in **4**, as well as both analogous bonds in **3a**. This bond is likely elongated by the increased  $\pi$ -accepting character of phen versus bpy. Both structures exhibit similar  $\pi$ - $\pi$  stacking motifs in the extended structure; both bpy and phen ligands in **3a** and **4**, respectively, have one *face-to-face* stacking interaction between two molecules and involving the entire ligands (both rings for bpy and all three rings in phen (Figures S87 and S99). On the other face, only one ring forms a *face-to-face* stacking interaction with one ring of the ligand in a third, adjacent molecule.

The single crystal X-ray diffraction structures of the other bpy adducts **3b** and **3c** are shown in Figure 3. The imido bond angles in **3b** are significantly larger than the same angles in **3c** due to the formation of the imide-containing metalocycle in **3c** (Table 1). Bent imido ligands typically contribute less electron

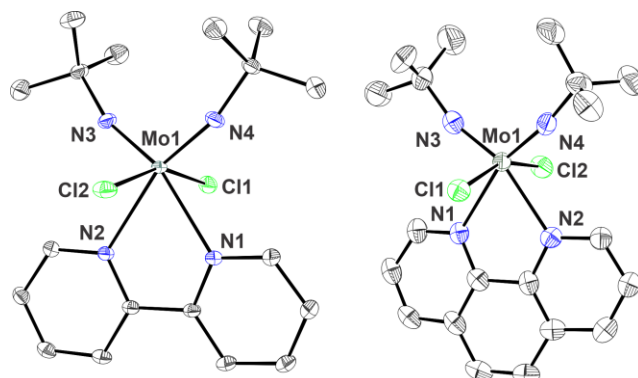


**Figure 2.** Solid-state structure of (*t*BuN)<sub>2</sub>MoCl<sub>2</sub>-bpy **3a** (left) and (*t*BuN)<sub>2</sub>MoCl<sub>2</sub>-phen **4** (right). Thermal ellipsoids are drawn at the 50% probability level. Hydrogen atoms have been omitted for visual clarity. The *tert*-butyl group (on N4) in **4** is disordered over two positions, however, only Part A of the disorder is shown for visual clarity.

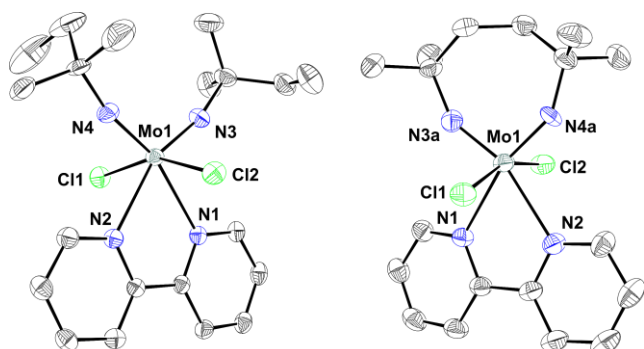


**Figure 3.** Solid-state structure of  $(t\text{BuN})_2\text{MoCl}_2\cdot\text{bpy}$  **3b** (left) and  $(\text{NCMe}_2(\text{CH}_2)_2\text{CMe}_2\text{N})\text{MoCl}_2\cdot\text{bpy}$  **3c** (right). Thermal ellipsoids are drawn at the 50% probability level. Hydrogen atoms have been omitted for visual clarity. The *tert*-pentyl group (on N4) in **3b**, and the entire ring comprising N3 and N4 in **3c**, are disordered over two positions, however, only Part A of the disorders are shown for visual clarity. Compound **3c** also contains a  $\text{CH}_2\text{Cl}_2$  solvent molecule that has been omitted from the image for visual clarity.

density to the metal center than linear imido ligands,<sup>[53]</sup> so the molybdenum center in **3c** should be more electron deficient. However, the Mo–Cl bond lengths in **3c** are longer than those in **3b** which suggests **3c** has more electron density at the metal. Additionally, the metrical parameters of the bpy ligands in both structures are equivalent and both structures exhibit similar  $\pi$ - $\pi$  stacking motifs (Figures S93 and S96).

The solid-state structures of the two  $t\text{BuDAD}^{\text{H}}$  adducts **5** and **6** are shown in Figure 4. The structure of **6** was found to have two inequivalent molecules in the asymmetric unit. The metrical parameters of the  $t\text{BuDAD}^{\text{H}}$  ligands are identical in both structures **5** and **6** (Table 1). The Mo–N(1/2) bond lengths are slightly shorter in the mixed oxo-imido compound **6** likely due to its reduced steric congestion. Additionally, the Mo–N2 bond in **6**, which is *trans* to the oxo ligand, is slightly shorter than the Mo–N1 bond, likely due to a reduced *trans* donor effect compared to the imido. The bond lengths and angles of the imido ligands are similar between both structures, but are slightly longer and less linear in **5**, possibly because combined these imidos still donate more electron density to the Mo(VI) center than one imido and one oxo ligand do in **6**. It should also be noted that the tungsten analogue of **5** has been reported previously.<sup>[54]</sup>

Single crystal X-ray structural results of the two other DAD adducts **7** and **8** are shown in Figure 5. The structure of compound **7** contains two inequivalent molecules in the asymmetric unit. The Mo–N(1/2) bond lengths in **7** are shorter than the same bonds in **8** (Table 1), due to their different steric profiles. Despite the apparently stronger binding of  $t\text{PrDAD}^{\text{Me}}$  in **7** compared to that of  $t\text{BuDAD}^{\text{H}}$  in **8** the Mo–N(3/4) imido bond

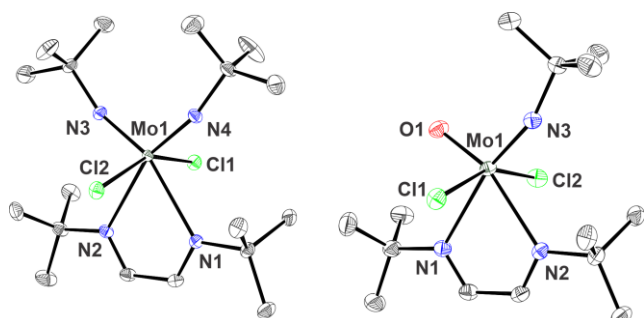


**Figure 4.** Solid-state structure of  $(t\text{BuN})_2\text{MoCl}_2\cdot(t\text{BuDAD})^{\text{H}}$  **5** (left) and  $(t\text{BuN})\text{MoOCl}_2\cdot(t\text{BuDAD})^{\text{H}}$  **6** (right). Thermal ellipsoids are drawn at the 50% probability level. Hydrogen atoms have been omitted for visual clarity. There are two molecules in the asymmetric unit of **6**, however, only molecule 1 is shown for visual clarity.

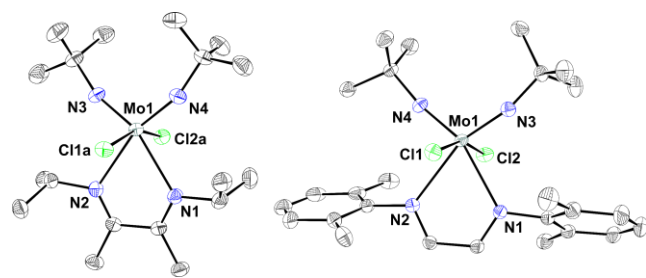


**Figure 5.** Solid-state structure of  $(t\text{BuN})_2\text{MoCl}_2\cdot(t\text{PrDAD})^{\text{Me}}$  **7** (left) and  $(t\text{BuN})_2\text{MoCl}_2\cdot(t\text{BuDAD})^{\text{H}}$  **8** (right). Thermal ellipsoids are drawn at the 50% probability level. Hydrogen atoms have been omitted for visual clarity. There are two molecules in the asymmetric unit of **7**, however, only molecule 1 is shown for visual clarity.

lengths are equivalent. However, the Mo–N(3/4)–C imido bond angles are more linear in **8** than in **7** suggesting that **8** has a stronger imido ligand contribution.<sup>[53]</sup>

Finally, we analyzed the single crystal X-ray structures of the two compounds incorporating hybrid-ligands: the impy adduct **9** and the dmampy adduct **10** (Figure 6). Most of the atoms in **9** are disordered over two sites with the imido ligands and the impy chelate occupying the same sites (see SI for details). Interestingly, the metrical parameters of both compounds are very similar, despite their having different chelating ligands. For example, the average imido bond lengths and angles are statistically equivalent in both structures (Table 1). Additionally, the *average* Mo–N(1/2) bond lengths are equivalent in both structures. However, the individual bond lengths are different, for example the Mo–N1 (pyridyl) bond length in both structures are significantly shorter than the Mo–N2 bond lengths, due the stronger bonding of the pyridyl rings. Incorporation of the pyridyl ring also results in both structures containing notable  $\pi$ - $\pi$  stacking interactions (Figures S110 and S113).

The most significant intermolecular interactions in these compounds fall into two main groups. The first group includes  $\pi$ - $\pi$  stacking and such interactions are found in every structure where it is possible for the aromatic rings of the ligand to align to do so. Stacking has been discussed for the individual compounds above, and only in **8** is an aromatic ring present without stacking observed. In the case of **8** the aromatic xylene rings are not bonded to Mo directly but rather are found as external groups on the central ring. This gives them a conformational flexibility not found in other compounds and, together with the *ortho*-methyl groups bonded to the xylene ring, prevents stacking interactions from forming in this one specific case.

The second type of intermolecular interaction found in all of these compounds is C–H...Cl hydrogen bonding (augmented by

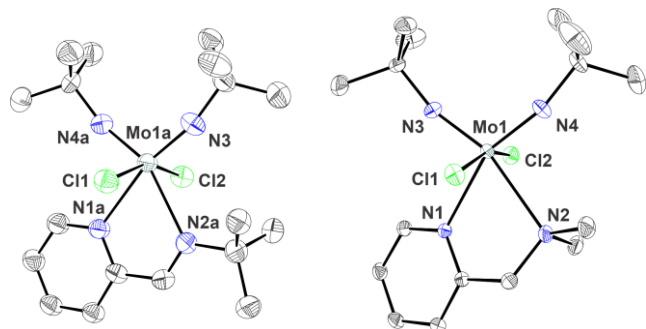


**Figure 6.** Solid-state structure of  $(t\text{BuN})_2\text{MoCl}_2\cdot\text{impy}$  **9** (left) and  $(t\text{BuN})_2\text{MoCl}_2\cdot\text{dmampy}$  **10** (right). Thermal ellipsoids are drawn at the 50% probability level. Hydrogen atoms have been omitted for visual clarity. Most of the molecule in **9** is disordered over two positions (see SI), however, only part A of the disorder is shown for visual clarity.

C–H...O contacts in **6**). The C–H...Cl contacts themselves fall into two main groups. In the compounds with  $\pi$ - $\pi$  stacking interactions, the strongest C–H...Cl contacts involve the same molecules interacting *via* the stacking arrangement. The Cl acceptor on one molecule will participate in hydrogen bonds with aromatic C–H donor groups from the rings involved with stacking on a second molecule (Figure S88). In those molecules where there is no  $\pi$ - $\pi$  stacking the C–H...Cl interactions are apparently more randomly formed. The Cl atoms still accept hydrogen bonds but with whichever C–H groups on the donor molecules that can approach most closely, generally from above and below the Cl–Mo–Cl axis (Figure S84).

Based on the crystallographic results, we expect the compounds that contain  $\pi$ - $\pi$  stacking interactions to have lower volatilities compared to those where such interactions are absent. This will also be true and important when considering the compounds containing only C–H...Cl hydrogen bonds; the stronger these bonds the less volatile the compound should be. Of course, C–H...Cl bonds are also found, and must be considered, in the aromatic structures.

#### Volatility and Thermal Stability: Effect of the Chelate Ligand

With our new family of *bis*(alkylimido)molybdenum(VI) precursor candidates in hand, we began experiments to evaluate their volatility and thermal stability. The volatility of the compounds was assessed using thermogravimetric analysis (TGA), from which the vapor pressure was also estimated based on the first derivative of the mass loss curve.<sup>[55,56]</sup> Herein  $T_V$  refers to the temperature at which 1 Torr of vapor pressure was achieved; this is a commonly desired pressure for ALD and CVD precursors. We also probed the thermal stability of the compounds by analysis of the residual mass from the TGA experiment. This was further investigated using a “thermal stress test”,<sup>[57]</sup> where the kinetics of the evaporation process were exploited. The thermal stability of each compound was also investigated using differential scanning calorimetry (DSC). Herein  $T_D$  refers to the onset of decomposition, which is defined as a 5% increase of the major exothermic process measured by DSC. All thermal data obtained from TGA, DSC, and from simple sublimation experiments are compiled in Table 2.

We wanted to further probe the volatility and thermal stability of the previously reported *tmeda* adduct, (<sup>t</sup>BuN)<sub>2</sub>MoCl<sub>2</sub>-*tmeda* **2a**. Thermogravimetric analysis showed that **2a** volatilizes well (Figure 7), with the onset of mass loss at ~140 °C. It had an onset of decomposition of 174 °C by DSC (Figure 8). Only 9% of **2a** had volatilized at this temperature in the ramped TGA experiment, so it must have been slowly decomposing while evaporating during this mass-loss event, which was the reason for the residual mass of 7%. Compound **2a** was further analyzed using isothermal TGA, which showed that the entirety of the sample evaporated at 140 °C and 170 °C with rates of evaporation of 54 and 580  $\mu\text{g min}^{-1}\text{cm}^{-2}$ , respectively (Figure S6). Thus, **2a** is a volatile compound with promise for ALD, provided it is kept below its  $T_D$  (174 °C).

The *bpy* adduct **3a** was also reinvestigated to gain insight into the superior thermal stability it had previously exhibited.<sup>[33]</sup> Ramped TGA showed that **3a** volatilized completely (Figure 7), and the  $T_V$  was estimated to be 249 °C (Table 2). DSC showed the compound to be very thermally stable with an onset of decomposition of 272 °C (Figure 8). This compound exhibited a moderate thermal range ( $\Delta T = T_V - T_D = 23$  °C)<sup>[58]</sup> so we performed a thermal stress test to determine if **3a** was kinetically

**Table 2.** Important thermal properties obtained from TGA, DSC, and sublimation.

Compound	$T_V$ / °C	$T_D$ / °C	Residual mass / %	$T_{\text{sub}}^{[a]}$
<b>2a</b>	173	174	7.0	145 <sup>[b]</sup>
<b>2b</b>	164	163	8.7	<sup>[c]</sup>
<b>2c</b>	186	182	17.7	<sup>[c]</sup>
<b>2d</b>	<sup>[d]</sup>	176	35.8	<sup>[c]</sup>
<b>3a</b>	249	272	0.0	200
<b>3b</b>	237	259	0.7	180
<b>3c</b>	255	220 <sup>[e]</sup>	8.4	200
<b>4</b>	303	302	30.3	230
<b>5</b>	135	170	2.0	95
<b>6</b>	175	183	24.2	130
<b>7</b>	<sup>[d]</sup>	108	40.7	<sup>[c]</sup>
<b>8</b>	179	155	6.3	160 <sup>[b]</sup>
<b>9</b>	199	232	0.0	170
<b>10</b>	200	200	35.3	170

[a] Sublimation temperature at 40 mTorr. [b] Sublimed with decomposition. [c] Decomposed upon heating. [d]  $T_V$  could not be estimated due to multiple mass-loss events in the TGA. [e] Inconsistent with the  $T_D$  estimated by isothermal analysis (ca. 240–250 °C, see Figure S20).

stable (Figure S14). Upon increasing the mass-loading from 10 mg to 20 mg, the residual mass increased from 0.0% to 8.7%, and a 40 mg mass loading resulted in a residual mass of 21.8%. Clearly, the *bpy* adduct **3a** does not fully evaporate before it undergoes decomposition: when the bulk of the mass experiences higher temperatures, decomposition becomes obvious. Isothermal TGA of **3a** showed that the sample evaporates entirely, when run at several temperatures between 200 and 250 °C (Figure S15).

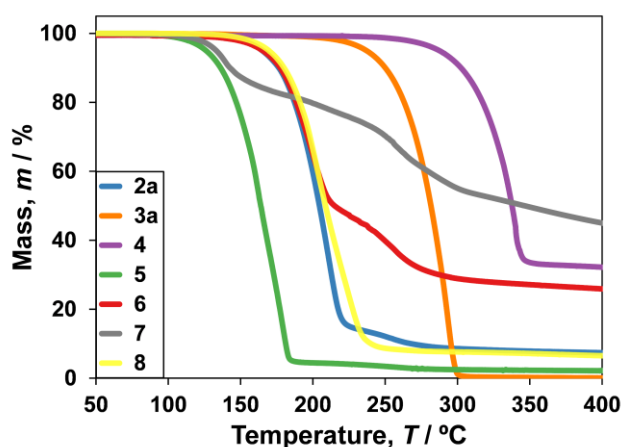


**Figure 7.** Thermogravimetric analyses of the (<sup>t</sup>BuN)<sub>2</sub>MoCl<sub>2</sub> adducts: (<sup>t</sup>BuN)<sub>2</sub>MoCl<sub>2</sub>-*tmeda* (**2a**, blue), (<sup>t</sup>BuN)<sub>2</sub>MoCl<sub>2</sub>-*bpy* (**3a**, orange), (<sup>t</sup>BuN)<sub>2</sub>MoCl<sub>2</sub>-*phen* (**4**, purple), (<sup>t</sup>BuN)<sub>2</sub>MoCl<sub>2</sub>-(<sup>t</sup>BuDAD<sup>H</sup>) (**5**, green), (<sup>t</sup>BuN)MoOCl<sub>2</sub>-(<sup>t</sup>BuDAD<sup>H</sup>) (**6**, red), (<sup>t</sup>BuN)<sub>2</sub>MoCl<sub>2</sub>-(<sup>t</sup>BuDAD<sup>Me</sup>) (**7**, grey), and (<sup>t</sup>BuN)<sub>2</sub>MoCl<sub>2</sub>-(<sup>t</sup>BuDAD<sup>H</sup>) (**8**, yellow). A heating rate of 10 °C min<sup>-1</sup> was used for all experiments, and the mass loadings were 10.0 ± 0.1 mg for each sample.

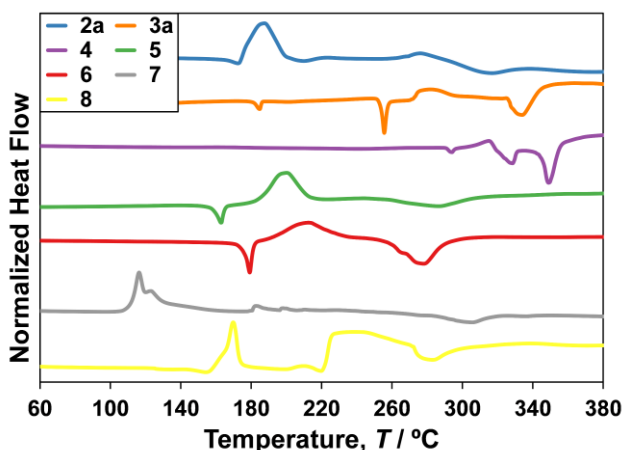


**Figure 8.** Differential scanning calorimetry plots of the  $(t\text{BuN})_2\text{MoCl}_2$  adducts:  $(t\text{BuN})_2\text{MoCl}_2\text{-tmeda}$  (**2a**, blue),  $(t\text{BuN})_2\text{MoCl}_2\text{-bpy}$  (**3a**, orange),  $(t\text{BuN})_2\text{MoCl}_2\text{-phen}$  (**4**, purple),  $(t\text{BuN})_2\text{MoCl}_2\text{-}({}^{\text{tBu}}\text{DAD}^{\text{H}})$  (**5**, green),  $(t\text{BuN})\text{MoOCl}_2\text{-}({}^{\text{tBu}}\text{DAD}^{\text{H}})$  (**6**, red),  $(t\text{BuN})_2\text{MoCl}_2\text{-}({}^{\text{Pr}}\text{DAD}^{\text{Me}})$  (**7**, grey), and  $(t\text{BuN})_2\text{MoCl}_2\text{-}({}^{\text{xy}}\text{DAD}^{\text{H}})$  (**8**, yellow). A heating rate of  $10\text{ }^\circ\text{C min}^{-1}$  was used for all experiments.

Thermogravimetric analysis of **4** resulted in a high residual mass of 30.3% (Figure 8). The derivative of the mass loss curve showed that this compound undergoes a single-step mass loss event (Figure S21). An isothermal TGA at the temperature showing 1% mass loss ( $255\text{ }^\circ\text{C}$ ) also resulted in a high residual mass, suggesting that the mass loss event is from decomposition and not volatilization. In a sublimation experiment, **4** sublimed intact with good yield ( $230\text{ }^\circ\text{C}$ , 40 mTorr), showing it is volatile at reduced pressure, which allows evaporation well before its high onset of decomposition ( $303\text{ }^\circ\text{C}$ ). This is further evidence that heteroaromatic ligands improve the thermal stability of the  $(t\text{BuN})_2\text{MoCl}_2$  moiety.

Ramped TGA of the  ${}^{\text{tBu}}\text{DAD}^{\text{H}}$  adduct **5** revealed the compound to be very volatile, resulting in a single-step volatilization and leaving a negligible residual mass (Figure 7). From the TGA it was also found that **5** has a low  $T_V$  ( $135\text{ }^\circ\text{C}$ ). A thermal stress test of **5** resulted in an appreciable increase of the residual mass (10.7%, Figure S24); volatility and thermal decomposition must overlap in the temperature range tested. Isothermal TGA experiments showed that **5** readily evaporates at isothermal temperatures between 105 and  $165\text{ }^\circ\text{C}$  with rates of evaporation of  $67$  and  $2100\text{ }\mu\text{g min}^{-1}\text{ cm}^{-2}$ , respectively (Figure 9). Additionally, it was found that **5** cleanly sublimes, without loss of its ligand, with good recovery at  $95\text{ }^\circ\text{C}$  (40 mTorr, 5 g scale).

The  ${}^{\text{tBu}}\text{DAD}^{\text{H}}$  adduct **5** was the most volatile  $(t\text{BuN})_2\text{MoCl}_2$  compound we had prepared, and so we wanted to see if we could further enhance the volatility by introducing other substituents onto the diazabutadiene ligand. TGA of the  ${}^{\text{Pr}}\text{DAD}^{\text{Me}}$  adduct **7** revealed multiple mass loss events, leading to a high residual mass of 40.7% (Figure 7). The first event begins at  $105\text{ }^\circ\text{C}$ , which directly corresponds to a sharp exotherm ( $T_D$ ) measured by DSC (Figure 8) and results in a mass loss of about 8%. Initially this was speculated to be a ligand-centered decomposition, forming propene (calcd. 9% mass-loss) via  $\beta$ -H abstraction from the isopropyl group, however, propene was not detected using *ex situ* methods (such as NMR and HRMS). We then speculated that this could have been from the elimination of HCl (calcd. 8% mass-loss). To further support this idea, we prepared the 1,4-dicyclopentyl-1,3-diazabutadiene ( ${}^{\text{cPe}}\text{DAD}^{\text{H}}$ ) adduct, which is analogous to **7** (in the sense that it also contains  $\beta$ -H atoms, see SI for details). TGA of the  ${}^{\text{cPe}}\text{DAD}^{\text{H}}$  adduct also resulted in a mass-

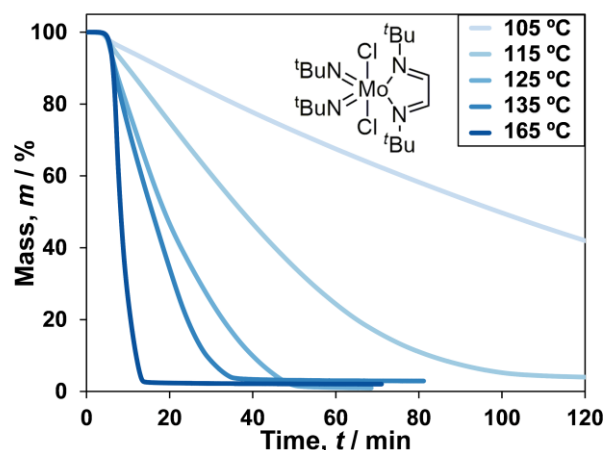
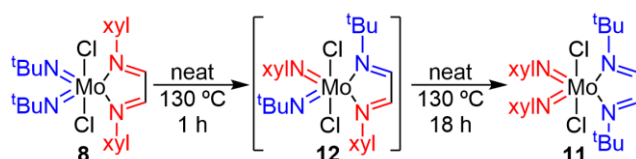


**Figure 9.** Isothermal analysis of  $(t\text{BuN})_2\text{MoCl}_2\text{-}({}^{\text{tBu}}\text{DAD}^{\text{H}})$  (**5**), using TGA. The samples were heated at  $20\text{ }^\circ\text{C min}^{-1}$  and then were held at the designated isothermal temperature. The mass loadings were  $10.0 \pm 0.1\text{ mg}$  for each sample.

loss event at  $113\text{ }^\circ\text{C}$  which corresponded to a sharp exotherm in its DSC curve. This results in a mass-loss of 7%, which does correspond to the elimination of HCl (calcd. 7%), whereas loss of cyclopentene would be larger (14%). Similar thermally induced  $\beta$ -H migrations (to ancillary ligands; Cl in the case of **7**) have been observed in 1,4-di-isopropyl-1,3-diazabutadiene complexes of Hf,<sup>[59]</sup> Ru,<sup>[60]</sup> and Fe.<sup>[61]</sup>

Since we had shown that incorporation of aryl groups into ligands is not entirely detrimental for volatility, and Pugh *et al.* had also shown that aryl-substituted diazabutadienes can be used as ligands in thermally stable cyclopentadienyl-cobalt(III) compounds,<sup>[39]</sup> we investigated the volatility of the  ${}^{\text{xy}}\text{DAD}^{\text{H}}$  adduct **8**. TGA of **8** resulted in a  $T_V$  of  $179\text{ }^\circ\text{C}$ , with a residual mass of 6.3% (Figure 7). The residual mass results from decomposition that occurs before complete evaporation, which is corroborated by the  $T_D$  of  $155\text{ }^\circ\text{C}$  (Figure 8). The TGA showed very little evaporation of **8** before the  $T_D$  (2% mass loss) suggesting that the decomposition product is also volatile. When the heating rate of the TGA was reduced from the standard  $10\text{ }^\circ\text{C min}^{-1}$  to  $5\text{ }^\circ\text{C min}^{-1}$  the residual mass decreased to 3.8% (Figure S30) because more of the material could evaporate prior to reaching the  $T_D$ .

The DSC curve of the  ${}^{\text{xy}}\text{DAD}^{\text{H}}$  adduct **8** also showed a low temperature decomposition that did not correspond to  $\gamma$ -H activation of the *tert*-butylimido ligands. To gain further insight into this decomposition we performed a solid-state thermolysis reaction of **8** ( $120\text{ }^\circ\text{C}$ , 18 hours, see SI for details). The residue was then analyzed using EI-HRMS and a molecular ion corresponding to  $(\text{xyN})_2\text{MoCl}_2^+$  was identified as the major component. A fragment corresponding to  ${}^{\text{tBu}}\text{DAD}^{\text{H}}$  was also observed, both in the EI-HRMS and by  ${}^1\text{H}$  NMR analysis. Additionally,  $(\text{xyN})_2\text{MoCl}_2\text{-dme}$  was treated with  ${}^{\text{tBu}}\text{DAD}^{\text{H}}$  (see SI) and the  ${}^1\text{H}$  NMR spectrum matched the residue from the thermolysis of **8** (Figure S1). This suggests that the thermolysis of **8** results in the formation of  $(\text{xyN})_2\text{MoCl}_2\text{-}({}^{\text{tBu}}\text{DAD}^{\text{H}})$  (**11**, Scheme



**Scheme 6.** Solid-state thermolysis of  $(t\text{BuN})_2\text{MoCl}_2\text{-}({}^{\text{xy}}\text{DAD}^{\text{H}})$  (**8**) resulting in the formation of  $(\text{xyN})_2\text{MoCl}_2\text{-}({}^{\text{tBu}}\text{DAD}^{\text{H}})$  (**11**).

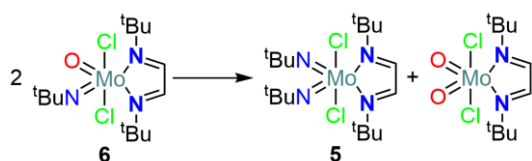
6); an intermediate species **12** was also detected (alongside **11**) using EI-HRMS when the reaction was run for only 1 hour. The decomposition of the  $^{99}\text{DAD}^{\text{H}}$  adduct **8** into **11** likely proceeds through imine metathesis with the diazabutadiene fragment ( $\text{RN}=\text{CHR}'$ ).<sup>[62–64]</sup> Finally, EI-HRMS of **8** did not show any of these ions, confirming that the imido exchange was not a result of ionization.

Finally, the thermal properties of the mixed oxo-imido  $^{\text{tBu}}\text{DAD}^{\text{H}}$  adduct **6** were also studied, and it appears to have a multi-step mass loss curve by TGA (Figure 7). The nature of the first mass loss, beginning at 130 °C, is unclear, but the second (beginning around 210 °C) is clearly decomposition, leading to a residual mass of 24.2%. The second mass loss was corroborated by DSC analysis (Figure 8) which showed **6** to have a  $T_{\text{D}}$  of 183 °C. To determine if the first mass loss event was in fact due to volatility, isothermal TGA experiments were conducted below the  $T_{\text{D}}$  of **6**, at 150 °C, 160 °C, and 170 °C. Interestingly, residual masses between 38.9 and 22.1% were observed, demonstrating that this compound starts to decompose at low temperature (Figure S130).  $^1\text{H}$  NMR analysis of the residual mass (a blue solid) revealed it to be  $\text{MoO}_2\text{Cl}_2 \cdot (^{\text{tBu}}\text{DAD}^{\text{H}})$ . This finding suggests that the oxo-imido compound **6** undergoes a retrosynthetic conversion to the *bis*(*tert*-butylimido)  $^{\text{tBu}}\text{DAD}^{\text{H}}$  adduct **5** and  $\text{MoO}_2\text{Cl}_2 \cdot (^{\text{tBu}}\text{DAD}^{\text{H}})$  (Scheme 7). We have already shown that **5** is volatile, and therefore upon its formation, it evaporates from the decomposition mixture. The higher residual mass from the lower temperature isothermal experiment is rationalized by the fact that lower temperatures require longer evaporation times, meaning the oxo-imido compound **6** has more time to dissociate before it has completely evaporated. As a supplemental study we have shown that  $\text{MoO}_2\text{Cl}_2 \cdot (^{\text{tBu}}\text{DAD}^{\text{H}})$  does not exhibit any volatility, with a decomposition mass loss occurring at 170 °C (see SI). This further supports the fact that *tert*-butylimido ligands provide great frameworks for volatility and incorporating one in **6** improves its volatility (compared to  $\text{MoO}_2\text{Cl}_2 \cdot (^{\text{tBu}}\text{DAD}^{\text{H}})$ ).

Compound **5** is the most volatile compound we report, and it also has an excellent thermal range. Therefore, this would be the best compound to explore further in ALD experiments. The observed oxo-imido exchange is an important finding since compound **6** demonstrates what a key intermediate in the gas-surface reaction between **5** and a metal oxide surface might look like. Similar reactions may also have occurred during the ALD of  $\text{MoO}_3$  with the  $(^{\text{tBu}}\text{N})_2\text{MoX}_2$  precursors **A** and **B** (Chart 1).<sup>[3,13,14]</sup>

### Volatility and Thermal Stability: Effect of the Alkyl Substituents

Following our investigation of the  $(^{\text{tBu}}\text{N})_2\text{MoCl}_2$  adducts, and how the addition of various *N,N'*-chelates affected their volatility and thermal stability, we decided to synthesize and study related alkyl imido substituted compounds. To probe the effect of manipulating this part of the molecule, we only prepared the *tmeda* and *bpy* adducts, as these ligands showed good volatility



**Scheme 7.** Thermally induced retrosynthetic conversion of  $(^{\text{tBu}}\text{N})\text{MoOCl}_2 \cdot (^{\text{tBu}}\text{DAD}^{\text{H}})$  **6** into  $(^{\text{tBu}}\text{N})_2\text{MoCl}_2 \cdot (^{\text{tBu}}\text{DAD}^{\text{H}})$  **5** and  $\text{MoO}_2\text{Cl}_2 \cdot (^{\text{tBu}}\text{DAD}^{\text{H}})$ .

and thermal stability (when coordinated to  $(^{\text{tBu}}\text{N})_2\text{MoCl}_2$ ), and those adducts were straightforward to synthesize.

We began by making the *tert*-pentyl analogues **2b** and **3b**. *A priori* we expected that the *tert*-pentyl analogue **2b** would be more volatile compared to **2a**, due its more numerous steric interactions, which would reduce intermolecular interactions.<sup>[65]</sup> From the TGA, **2b** was found to have a lower onset of the thermal feature (108 °C) than **2a**, with a similar residual mass (Figure 10, Table 2). From DSC it was found that **2b** had a lower  $T_{\text{D}}$  (163 °C, Figure 11) than **2a**, possibly due to  $\gamma$ -H elimination. This would give a more stable product, an internal alkene (2-methyl-2-butylene), resulting in a more exergonic process (discussed below with Scheme 8).

In contrast to **2b**, the *bpy* adduct **3b** showed remarkable improvements, relative to **3a**. For example, ramped TGA of **3b** resulted in complete evaporation, with a negligible residual mass (0.7%), and a  $T_{\text{V}}$  of 237 °C (12 °C lower than **3a**). Its onset of decomposition (259 °C) was slightly lower than that of **3a**. Isothermal TGA showed that **3b** evaporated without decomposition between 190 and 260 °C, sufficient volatilization to warrant using it as an ALD precursor. Clearly *tert*-pentyl substitution offers improved volatility compared to *tert*-butyl, but at the cost of reduced thermal stability. Due to the chemical similarities between *tert*-butyl and *tert*-pentyl, other compounds related to those in Chart 1 could be easily prepared by substituting *tert*-pentyl imidos for the *tert*-butyl groups, which should result in improved volatilities over those of the known precursors.

The *tert*-pentyl compounds appear to exhibit similar decomposition pathways to those of the *tert*-butyl analogues. We attempted to block this primary decomposition pathway by tethering the imido groups together. In turn, we hoped that this would prevent a single-step decomposition, one that produces a very volatile by-product, which would slow the rate of decomposition and result in a higher  $T_{\text{D}}$ . Ramped TGA revealed the tethered imido adduct **2c** was not as volatile as **2a** (Figure 10), but it was more thermally stable ( $T_{\text{D}}$  of 182 °C for **2c** vs. 174 °C for **2a**, Figure 11). Despite the higher stability, a residual mass of 17.7% was observed in the ramped TGA of **2c** and there were two thermal events apparent in the TGA. The first event was likely a combination of evaporation and decomposition ( $\gamma$ -H elimination into a protio-imido) and the second higher temperature TGA

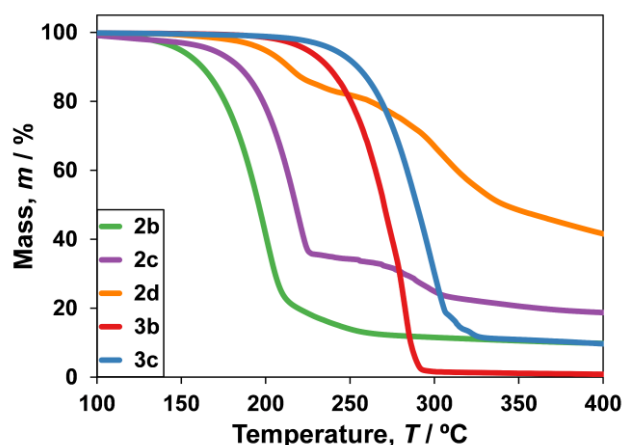


**Figure 10.** Thermogravimetric analyses of the alkylimido compounds:  $(^{\text{tBu}}\text{N})_2\text{MoCl}_2 \cdot \text{tmeda}$  (**2b**, green),  $(\text{NCMe}_2(\text{CH}_2)_2\text{CMe}_2\text{N})\text{MoCl}_2 \cdot \text{tmeda}$  (**2c**, purple),  $(\text{AdN})_2\text{MoCl}_2 \cdot \text{tmeda}$  (**2d**, orange),  $(^{\text{tBu}}\text{N})_2\text{MoCl}_2 \cdot \text{bpy}$  (**3b**, red),  $(\text{NCMe}_2(\text{CH}_2)_2\text{CMe}_2\text{N})\text{MoCl}_2 \cdot \text{bpy}$  (**3c**, blue). A heating rate of  $10\text{ °C min}^{-1}$  was used for all experiments, and the mass loadings were  $10.0 \pm 0.1\text{ mg}$  for each sample.

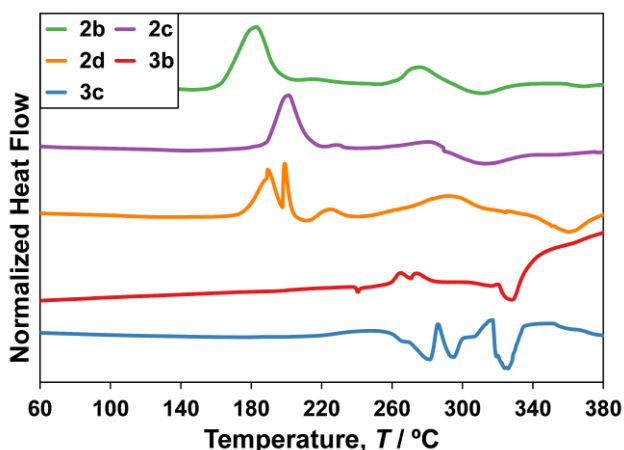
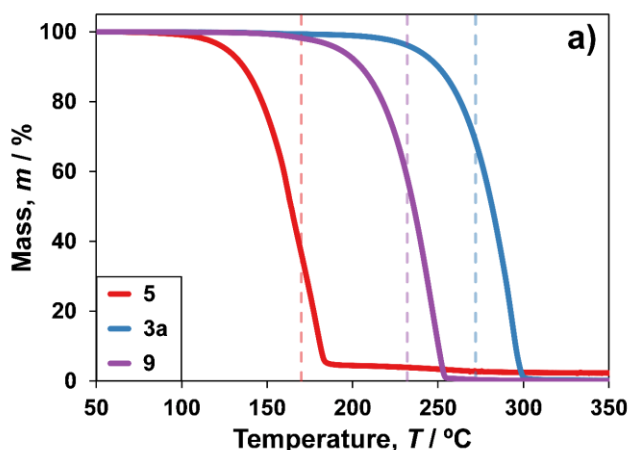


**Figure 11.** Differential scanning calorimetry plots of the alkylimido compounds:  $(^i\text{PrN})_2\text{MoCl}_2\text{-tmeda}$  (**2b**, green),  $(\text{NCMe}_2(\text{CH}_2)_2\text{CMe}_2\text{N})\text{MoCl}_2\text{-tmeda}$  (**2c**, purple),  $(\text{AdN})_2\text{MoCl}_2\text{-tmeda}$  (**2d**, orange),  $(^i\text{PrN})_2\text{MoCl}_2\text{-bpy}$  (**3b**, red),  $(\text{NCMe}_2(\text{CH}_2)_2\text{CMe}_2\text{N})\text{MoCl}_2\text{-bpy}$  (**3c**, blue). A heating rate of  $10\text{ }^\circ\text{C min}^{-1}$  was used for all experiments.

feature, occurring at  $\sim 230\text{ }^\circ\text{C}$ , was likely the decomposition of that resulting proto-imido species into  $\text{MoCl}_x\text{N}_y$ .<sup>[66]</sup> A similar feature was observed at the same temperature in the stress test of the unligated parent dimer,  $[(^i\text{BuN})\text{Mo}(\mu\text{-N}^i\text{Bu})\text{Cl}_2]_2$  (Scheme 8, *vide infra*).<sup>[33]</sup>

The properties of the tethered bpy adduct **3c** were similar to those of the other bpy adducts, with an estimated  $T_V$  of  $255\text{ }^\circ\text{C}$ , however TGA gave a residual mass of 8.4%. This is likely due to its “negative” thermal range, where it starts to decompose ( $220\text{ }^\circ\text{C}$  by DSC)  $35\text{ }^\circ\text{C}$  before its  $T_V$ . Despite this, **3c** completely evaporated during isothermal analyses between  $210$  and  $240\text{ }^\circ\text{C}$ . In the isothermal experiments decomposition was only observed above  $250\text{ }^\circ\text{C}$ , which suggests that the exothermic event observed for **3c** by DSC at  $220\text{ }^\circ\text{C}$  results in the formation of another volatile compound. Electron impact high resolution mass spectrometry (EI-HRMS) of **3c** revealed competing decomposition pathways, other than  $\gamma\text{-H}$  elimination. While the tethered imido appears to hinder the low-temperature  $\gamma\text{-H}$  activation, **3c** is likely less stable than **3a** due to an alternative higher-temperature decomposition pathway, exclusive to the  $\text{NCMe}_2(\text{CH}_2)_2\text{CMe}_2\text{N}$  ring; this pathway needs a more in-depth investigation.



Finally, the tmeda adducts all showed non-negligible residual masses and could not be sublimed without noticeable decomposition. To interrogate this decomposition, we investigated the 1-adamantylimido tmeda adduct **2d**. We expected that the substitution of *tert*-butyl groups by 1-adamantyl would improve thermal stability as the unstable bridgehead alkene, adamantene, would be formed upon  $\gamma\text{-H}$  elimination. Ramped TGA of **2d** showed that, although it was not volatile, the first mass-loss event beginning at  $150\text{ }^\circ\text{C}$  corresponded to the relative mass of tmeda in the parent molecule (ca. 20%, Figures 10 and S12). This suggests that the chelating ligands dissociate from the metal complex prior to decomposition. We could not observe the same phenomenon in the other tmeda adducts since their volatilization and decomposition occur at the same time and were not resolved by ramped TGA experiments.

### Combining Desirable Characteristics with Hybrid Ligands

Finally, we wanted to see if we could make “hybrid” ligands that would combine the desirable characteristics of two different ligands. The *tert*-butylimido compounds had provided the best overall results (with straight-forward ligands), and they were also the easiest to prepare, so we used the  $(^i\text{BuN})_2\text{MoCl}_2$  framework to explore this idea. To begin, we investigated the thermal properties of the impy adduct **9**, which has a pyridyl/imino hybrid ligand structure that we hoped would combine the volatility of the  $^i\text{BuDAD}^{\text{H}}$  adduct **5** with the thermal stability of the bpy adduct **3a**. Thermogravimetric analysis of **9** revealed that the compound completely evaporates without leaving a residue (Figure 12a). Analysis of the DSC plot also revealed that this compound is very thermally stable, with  $T_D$  of  $232\text{ }^\circ\text{C}$  (Table 2). Both the  $T_V$  and the  $T_D$  of the impy adduct **9** are almost exactly intermediate to those properties in compounds **3a** and **5**, clearly suggesting the pyridyl ring offers some thermal stabilization. This thermal enhancement was further observed in the stress test of **9** which resulted in a residual mass of only 5.3%, with a 40 mg mass-loading (Figure S34). Not only is the impy adduct **9** thermally stable, but it has improved volatility compared to the bpy adduct **3a**, with a  $T_V$  of  $199\text{ }^\circ\text{C}$  (Table 2). For example, isothermal TGA showed **9** evaporated without decomposition between  $165$  and  $225\text{ }^\circ\text{C}$  with rates between  $54$  and  $1920\text{ }\mu\text{g min}^{-1}\text{ cm}^{-2}$ , respectively (Figure S35). Additionally, we found that the impy adduct **9** cleanly sublimes, without noticeable decomposition or dissociation of the

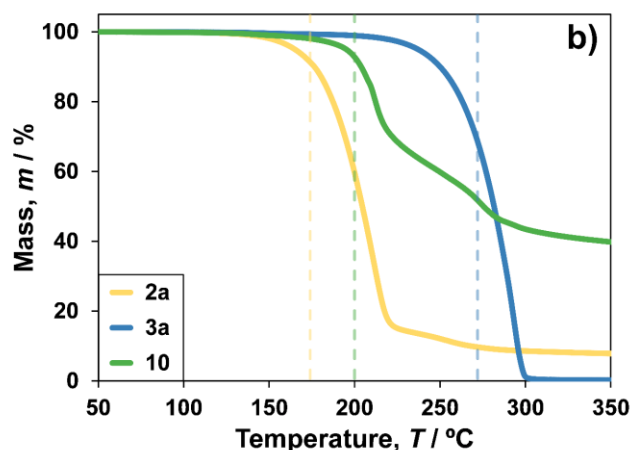
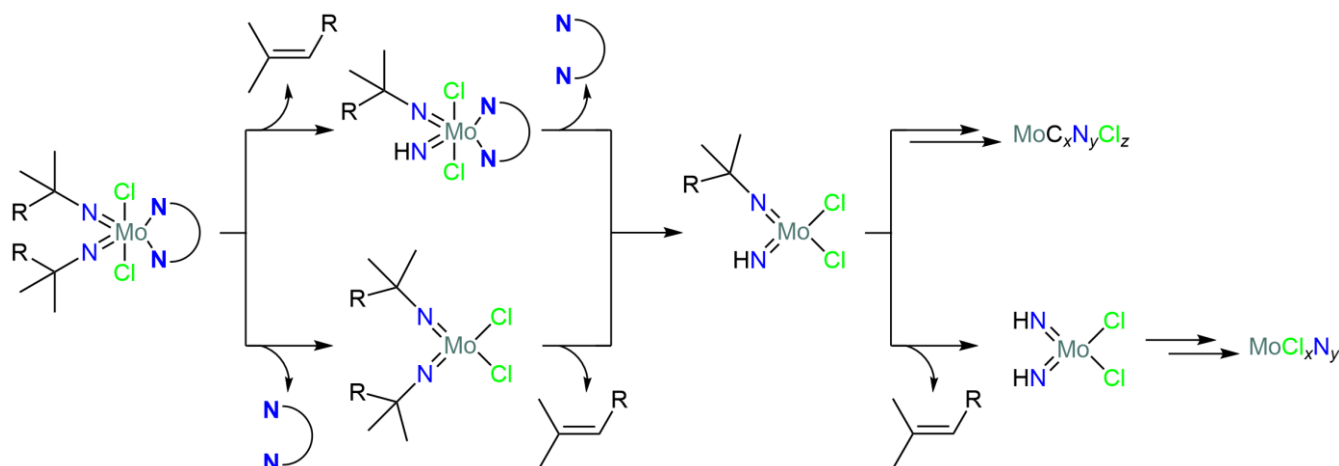


**Figure 12.** Thermogravimetric analyses of the compounds incorporating hybrid ligands,  $(^i\text{BuN})_2\text{MoCl}_2\text{-impy}$  (**9**) (a, left) and  $(^i\text{BuN})_2\text{MoCl}_2\text{-dmampy}$  (**10**) (b, right), highlighting their combination of characteristics. Vertical lines are also drawn at each compound's  $T_D$  to further emphasize the combination of properties from hybrid ligands. A heating rate of  $10\text{ }^\circ\text{C min}^{-1}$  was used for all experiments, and the mass loadings were  $10.0 \pm 0.1\text{ mg}$  for each sample. The DSC curves for **9** and **10** can be found in the SI.

ligand (170 °C, 40 mTorr). Clearly the impy adduct **9** is a successful example of hybrid ligand design.

Following the same hybrid ligand approach used in the preparation of compound **9**, we wanted to see if we could find a ligand that combined the properties of tmeda and bpy. Ramped TGA of the dmampy adduct **10** (which has a pyridyl/amino hybrid ligand) resulted in a multi-step mass loss curve leading to a residual mass of 35.3% (Figure 12b). This compound was found to have equivalent  $T_V$  and  $T_D$  of 200 °C, with both values between the corresponding values of the tmeda adduct **2a** and the bpy adduct **3a**. This further demonstrates the utility of the hybrid ligand concept, even when, as in this case, the thermal sensitivity is enhanced by the method. Despite **10** exhibiting poor thermal properties, it did sublime without noticeable decomposition (170 °C, 40 mTorr) suggesting it might be further tuned for greater thermal stability. Clearly hybrid ligands can be exploited to tune the frameworks discussed herein, to further optimize the structure and properties of ALD precursors.

Finally, analysis of the DSC curves of all of the compounds reported herein revealed two unique trends which provided insight into their mechanisms of decomposition (Figures 8 and 11). Immediately before the exothermic events, in the TGA of most of the compounds, is an endothermic event. This endothermic process is consistent with the dissociation of the  $N,N'$ -chelating ligand from the metal complex (Scheme 8), as was observed in **2d** (Figure 10). Attempts to quantify the enthalpy of these thermodynamic events did not result in reasonable values; this was likely due to the existence of multiple enthalpic events such as the dissociation of the ligand, melting of  $(t\text{-BuN})_2\text{MoCl}_2$ , and mixing of the components, confounding this simple analysis. Ultimately, these compounds likely decompose into  $\text{MoCl}_x\text{N}_y$  as we have previously observed.<sup>[33]</sup> Additionally, the DSC curves of all of the compounds reported herein contained noticeable endothermic processes after their exothermic events, ranging from 270 to 350 °C, which could be a phase change of the decomposition products. The shift in temperatures of the endotherms could be due to either ligation or different composition of the decomposition product (such as carbon content from the ligands, Scheme 8). Many of the thermal mechanisms reported herein require in-depth investigations, and we are continuing to explore the thermodynamics and kinetics of ligand dissociation,  $\gamma$ -H activation of the imido groups (Scheme 8), and ancillary ligand decomposition.



**Scheme 8.** Proposed pathways for the thermal decomposition of the  $(\text{RM}_2\text{N})_2\text{MoCl}_2\text{-L}$  ( $\text{L}$  = neutral  $N,N'$ -chelate) compounds. The mechanism does not account for potential ancillary ligand decompositions.

## Conclusion

A series of *bis*(alkyl-imido)-molybdenum(VI) compounds containing a variety of  $N,N'$ -chelates have been synthesized by ligand exchange reactions. All compounds have been structurally characterized using single-crystal X-ray crystallography. Their volatility has been assessed using TGA and the 1,4-di-*tert*-butyl-1,3-diazabutadiene adduct **5** was found to be the most volatile ( $T_V$  = 135 °C) and should therefore be further explored for use as a precursor in ALD. The thermal stability of these compounds was measured using DSC and the 1,10-phenanthroline adduct **4** was found to be the most stable, with an onset of decomposition of 303 °C. We also found that the utilization of hybrid ligands allowed us to customize thermal properties. This was highlighted by the synthesis of the *tert*-butyl(pyridine-2-yl-methyleneamine) (impy) adduct **9**, which was found to exhibit an excellent combination of volatility and thermal stability, as evidenced by low residual mass during a thermal stress test. Thermal testing of other alkyl-imido adducts revealed that these compounds undergo similar decomposition pathways. Despite their exhibiting good thermal stability, the mechanism of decomposition of all compounds should be further analyzed. This would contribute to the proper assessment of vapor deposition mechanisms using the  $(\text{RN})_2\text{MoCl}_2$  framework, a valuable source for the delivery of Mo to target films.

## Experimental Section

**Synthesis. General Experimental.** All manipulations were performed under air-free conditions using either standard Schlenk techniques or in a nitrogen-filled (99.998% purity) MBraun glovebox. 1,10-Phenanthroline ( $\geq 99\%$ ), was purchased from Sigma-Aldrich and was used as received. 1,4-Di-*tert*-butyl-1,3-diazabutadiene ( $^{\text{Bu}}\text{DADH}$ ),<sup>[67]</sup> 1,4-di-isopropyl-2,3-dimethyl-1,3-diazabutadiene ( $^{\text{P}}\text{DADMe}$ ),<sup>[68]</sup> 1,4-*bis*(2,6-dimethylphenyl)-1,3-diazabutadiene ( $^{\text{xy}}\text{DADH}$ ),<sup>[69]</sup> 1,4-dicyclopentyl-1,3-diazabutadiene ( $^{\text{Pp}}\text{DADH}$ ),<sup>[70]</sup> *tert*-butyl(pyridine-2-yl-methyleneamine) (impy),<sup>[71]</sup> 2-( $N,N$ -dimethylamino-methylpyridine) (dmampy),<sup>[72]</sup> 1-(*tert*-butylimino)- $N,N$ ,2-trimethylpropan-2-amine (imtpa),<sup>[45]</sup> 2,5-dimethylhexane-2,5-diamine,<sup>[73]</sup>  $(t\text{-BuN})_2\text{MoCl}_2\text{-dme}$  (**1a**),<sup>[34,35]</sup>  $(\text{PeN})_2\text{MoCl}_2\text{-dme}$  (**1b**),<sup>[48]</sup>  $(\text{NCMe}_2(\text{CH}_2)_2\text{CMe}_2\text{N})\text{MoCl}_2\text{-dme}$  (**1c**),<sup>[49]</sup>  $(\text{AdN})_2\text{MoCl}_2\text{-dme}$  (**1d**),<sup>[50]</sup>  $\text{MoO}_2\text{Cl}_2\text{-dme}$ ,<sup>[74]</sup>  $\text{MoO}_2\text{Cl}_2\text{-}^{\text{Bu}}\text{DADH}$ ,<sup>[38]</sup>  $(t\text{-BuN})\text{MoOCl}_2\text{-dme}$ ,<sup>[75]</sup>  $(t\text{-BuN})_2\text{MoCl}_2\text{-tmeda}$  (**2a**),<sup>[33]</sup>  $(t\text{-BuN})_2\text{MoCl}_2\text{-bpy}$  (**3a**),<sup>[33]</sup> and  $(xy\text{N})_2\text{MoCl}_2\text{-dme}$ <sup>[34]</sup> were all prepared following known methods, which are also described in the SI. All solvents (ACS reagent-grade) were

purified using a MBraun Solvent Purification System and were stored over 4 Å molecular sieves. All glassware was oven-dried at 130 °C, for at least 3 hours, prior to use. <sup>1</sup>H and <sup>13</sup>C{<sup>1</sup>H} NMR spectra were collected on a Bruker AVANCE 300 MHz spectrometer at room temperature and are referenced to residual solvent. Low temperature NMR spectra were collected on a Bruker AVANCE 500 MHz spectrometer, at the University of Ottawa. C<sub>6</sub>D<sub>6</sub> and CDCl<sub>3</sub> were purchased from Cambridge Isotope Laboratories, Inc. and were degassed using freeze-pump-thaw cycles prior to being stored over 4 Å molecular sieves under nitrogen. High-resolution mass spectra were collected on a Kratos Concept electron impact mass spectrometer, at the University of Ottawa. Elemental analyses (EA) were performed on a PerkinElmer 2400 combustion CHN analyser at the University of Windsor.

(*PeN*)<sub>2</sub>MoCl<sub>2</sub>-*tmeda* **2b**. *N,N,N',N'*-Tetramethylethylenediamine (0.235 g, 2.022 mmol) was added to a solution of the dme adduct **1b** (0.602 g, 1.409 mmol) in 10 mL of pentane. After stirring at room temperature for 2 hours the volatiles were removed *in vacuo* resulting in a waxy orange solid. The solid was dissolved in a minimal amount of pentane (ca. 2 mL) and was stored at -30 °C for 4 hours resulting in orange crystals. The mother liquor was decanted, and the crystals were dried *in vacuo*. The crystals were then dissolved in 10 mL of benzene which was subsequently frozen in liquid nitrogen, and removed by sublimation (lyophilization), resulting in a pale-orange powder. Yield = 0.403 g (0.889 mmol, 63%). <sup>1</sup>H NMR (300 MHz, C<sub>6</sub>D<sub>6</sub>, ppm): δ 1.09 (t, 6H, <sup>3</sup>J<sub>HH</sub> = 7.5 Hz, CH<sub>2</sub>CH<sub>3</sub>), 1.43 (s, 12H, C(CH<sub>3</sub>)<sub>2</sub>), 1.79 (q, 4H, <sup>3</sup>J<sub>HH</sub> = 7.5 Hz, CH<sub>2</sub>CH<sub>3</sub>), 2.08 (s, 4H, NCH<sub>2</sub>), 2.57 (s, 12H, N(CH<sub>3</sub>)<sub>2</sub>). <sup>13</sup>C{<sup>1</sup>H} NMR (75 MHz, C<sub>6</sub>D<sub>6</sub>, ppm): δ 9.83 (CH<sub>2</sub>CH<sub>3</sub>), 27.66 (C(CH<sub>3</sub>)<sub>2</sub>), 37.16 (CH<sub>2</sub>CH<sub>3</sub>), 50.59 (N(CH<sub>3</sub>)<sub>2</sub>), 57.27 (NCH<sub>2</sub>), 74.94 (C(CH<sub>3</sub>)<sub>2</sub>). Selected IR data (KBr, cm<sup>-1</sup>): ν(Mo=N) 1190 (vs), 1225 (s). EA calcd for C<sub>16</sub>H<sub>38</sub>Cl<sub>2</sub>MoN<sub>4</sub> [%]: C, 42.39; H, 8.45; N, 12.36; found [%]: C, 42.13; H, 8.78; N, 12.14.

NCMe<sub>2</sub>(CH<sub>2</sub>)<sub>2</sub>CMe<sub>2</sub>N)MoCl<sub>2</sub>-*tmeda* **2c**. *N,N,N',N'*-Tetramethylethylenediamine (0.141 g, 1.213 mmol) was added to a solution of the dme adduct **1c** (0.333 g, 0.838 mmol) in 10 mL of diethyl ether. After stirring at room temperature for 2 hours the volatiles were removed *in vacuo* resulting in a beige solid. The solid was dissolved in 1 mL of dichloromethane, layered with 1 mL of pentane, and was the resultant stored at -30 °C for 12 hours resulting in orange crystals. The mother liquor was decanted, and the crystals were washed with 2 mL of cold pentane. After drying *in vacuo* the product was isolated as an orange powder. Yield = 0.245 g (0.578 mmol, 69%). <sup>1</sup>H NMR (300 MHz, C<sub>6</sub>D<sub>6</sub>, ppm): δ 1.22 (s, 12H, C(CH<sub>3</sub>)<sub>2</sub>), 2.05 (s, 4H, NCH<sub>2</sub>), 2.51 (s, 12H, N(CH<sub>3</sub>)<sub>2</sub>), the CH<sub>2</sub> signal was not detected. <sup>1</sup>H NMR (500 MHz, CDCl<sub>3</sub>, -20 °C, ppm): δ 1.09 (s, 6H, C(CH<sub>3</sub>)<sub>2</sub>), 1.27 (s, 6H, C(CH<sub>3</sub>)<sub>2</sub>), 1.81 (d, 2H, <sup>3</sup>J<sub>HH</sub> = 11.3 Hz, CH<sub>2</sub>), 2.51 (m, 4H, NCH<sub>2</sub>), 2.61 (s, 12H, N(CH<sub>3</sub>)<sub>2</sub>), 2.90 (d, 2H, <sup>3</sup>J<sub>HH</sub> = 11.3 Hz, CH<sub>2</sub>). <sup>13</sup>C{<sup>1</sup>H} NMR (75 MHz, C<sub>6</sub>D<sub>6</sub>, ppm): δ 25.42 (br s, C(CH<sub>3</sub>)<sub>2</sub>), 41.26 (CH<sub>2</sub>), 50.20 (N(CH<sub>3</sub>)<sub>2</sub>), 56.89 (NCH<sub>2</sub>), 75.06 (C(CH<sub>3</sub>)<sub>2</sub>). Selected IR data (KBr, cm<sup>-1</sup>): ν(Mo=N) 1176 (vs), 1209 (s). EA calcd for C<sub>14</sub>H<sub>32</sub>Cl<sub>2</sub>MoN<sub>4</sub> [%]: C, 39.73; H, 7.62; N, 13.24; found [%]: C, 39.81; H, 7.56; N, 12.96.

(AdN)<sub>2</sub>MoCl<sub>2</sub>-*tmeda* **2d**. *N,N,N',N'*-Tetramethylethylenediamine (0.081 g, 0.697 mmol) was added to a slurry of the dme adduct **1d** (0.322 g, 0.580 mmol) in 10 mL of diethyl ether. After stirring at room temperature for 4 hours the volatiles were removed *in vacuo* resulting in an orange residue. This material was dissolved in 2 mL of dichloromethane, layered with 3 mL of pentane, and the resultant stored at -30 °C for 18 hours resulting in orange crystals. The mother liquor was decanted, and the crystals were washed with three, 2 mL portions of diethyl ether, and three, 2 mL portions of pentane. After drying *in vacuo*, the product was isolated as a pale-orange powder. Yield = 0.244 g (0.420 mmol, 72%). <sup>1</sup>H NMR (300 MHz, C<sub>6</sub>D<sub>6</sub>, ppm): δ 1.54 (m, 12H, CH<sub>2</sub> of Ad), 2.00 (m, 6H, CH of Ad), 2.17 (s, 4 H, NCH<sub>2</sub>), 2.24 (m, 12H, CH<sub>2</sub> of Ad), 2.67 (s, 12H, N(CH<sub>3</sub>)<sub>2</sub>). <sup>13</sup>C{<sup>1</sup>H} NMR (75 MHz, C<sub>6</sub>D<sub>6</sub>, ppm): δ 29.92 (CH of Ad), 36.55 (CH<sub>2</sub> of Ad), 43.61 (CH<sub>2</sub> of Ad), 50.82 (N(CH<sub>3</sub>)<sub>2</sub>), 57.29 (NCH<sub>2</sub>), 72.90 (Cq of Ad). Selected IR data (KBr, cm<sup>-1</sup>): ν(Mo=N) 1198 (s), 1236 (s). EA calcd for C<sub>26</sub>H<sub>46</sub>Cl<sub>2</sub>MoN<sub>4</sub>·0.33(CH<sub>2</sub>Cl<sub>2</sub>) [%]: C, 51.86; H, 7.71; N, 9.19; found [%]: C, 52.01; H, 7.55; N, 9.25.

(*PeN*)<sub>2</sub>MoCl<sub>2</sub>-*bpy* **3b**. 2,2'-Bipyridine (0.179 g, 1.146 mmol) was added to a solution of the dme adduct **1b** (0.446 g, 1.044 mmol) in 10 mL of diethyl ether. After stirring at room temperature for 2 hours the mixture was filtered through a sintered glass frit, and an orange solid was collected. The solid was washed with two, 2 mL portions of diethyl ether, and five, 3 mL portions of pentane. The solids were dried *in vacuo* resulting in an analytically pure pale-orange powder. Yield = 0.473 g (0.959 mmol, 92%). X-ray quality crystals were obtained after storing a saturated dichloromethane solution, layered with pentane, at -30 °C for 2 hours. <sup>1</sup>H NMR (300 MHz, C<sub>6</sub>D<sub>6</sub>, ppm): δ 1.29 (t, 6H, <sup>3</sup>J<sub>HH</sub> = 7.5 Hz, CH<sub>2</sub>CH<sub>3</sub>), 1.71 (s, 12H, C(CH<sub>3</sub>)<sub>2</sub>), 2.04 (q, 4H, <sup>3</sup>J<sub>HH</sub> = 7.5 Hz, CH<sub>2</sub>CH<sub>3</sub>), 6.67 (dd, 1H, J = 5.3 & 1.2 Hz), 6.69 (dd, 1H, J = 5.3 & 1.2 Hz), 6.90 (td, 2H, J = 7.8 & 1.8 Hz), 7.05 (dt, 2H, J = 8.0 & 0.9 Hz), 9.56 (dq, 2H, J = 5.3 & 0.9 Hz). <sup>13</sup>C{<sup>1</sup>H} NMR (75 MHz, C<sub>6</sub>D<sub>6</sub>, ppm): δ 10.01 (CH<sub>2</sub>CH<sub>3</sub>), 28.52 (C(CH<sub>3</sub>)<sub>2</sub>), 37.77 (CH<sub>2</sub>CH<sub>3</sub>), 74.70 (C(CH<sub>3</sub>)<sub>2</sub>), 121.44, 124.78, 138.12, 150.92, 152.79. Selected IR data (KBr, cm<sup>-1</sup>): ν(Mo=N) 1192 (s), 1221 (m). EA calcd for C<sub>20</sub>H<sub>30</sub>Cl<sub>2</sub>MoN<sub>4</sub> [%]: C, 48.69; H, 6.13; N, 11.36; found [%]: C, 48.67; H, 5.77; N, 11.26.

(NCMe<sub>2</sub>(CH<sub>2</sub>)<sub>2</sub>CMe<sub>2</sub>N)MoCl<sub>2</sub>-*bpy* **3c**. 2,2'-Bipyridine (0.230 g, 1.473 mmol) was added to a solution of the *tmeda* adduct **2c** (0.575 g, 1.358 mmol) in 10 mL of diethyl ether. After stirring at room temperature for 4 hours, 3 mL of pentane was added to the mixture to facilitate the precipitation of the product. The mixture was filtered through a sintered glass frit and the solids were washed with three, 3 mL portions of pentane. The resulting yellow-beige solids were dissolved in 5 mL of dichloromethane, layered with 1 mL of hexane, and the resultant stored at -30 °C for 18 hours resulting in yellow crystals. The mother liquor was decanted, and the crystals were washed with three, 3 mL portions of pentane and dried *in vacuo*, resulting in a yellow powder (Note: <sup>1</sup>H NMR analysis revealed the sample contained CH<sub>2</sub>Cl<sub>2</sub> which took 12-18 hours to completely remove *in vacuo*). Yield = 0.471 g (1.017 mmol, 75%). <sup>1</sup>H NMR (300 MHz, CDCl<sub>3</sub>, ppm): δ 1.39 (s, 12H, C(CH<sub>3</sub>)<sub>2</sub>), 2.55 (br s, 4H, CH<sub>2</sub>), 7.53 (t, 2H, J = 6.3 Hz), 7.95 (s, 2H, J = 7.6 Hz), 8.09 (d, 2H, J = 7.9 Hz), 9.28 (d, 2H, J = 4.5 Hz). <sup>13</sup>C{<sup>1</sup>H} NMR (75 MHz, CDCl<sub>3</sub>, ppm): δ 26.60 (br s, C(CH<sub>3</sub>)<sub>2</sub>), 41.67 (CH<sub>2</sub>), 75.55 (C(CH<sub>3</sub>)<sub>2</sub>), 122.00, 125.89, 139.30, 150.74, 152.35. Selected IR data (KBr, cm<sup>-1</sup>): ν(Mo=N) 1176 (vs), 1209 (s). EA calcd for C<sub>18</sub>H<sub>24</sub>Cl<sub>2</sub>MoN<sub>4</sub> [%]: C, 46.67; H, 5.22; N, 12.09; found [%]: C, 46.44; H, 4.71; N, 11.91.

(*BuN*)<sub>2</sub>MoCl<sub>2</sub>-*phen* **4**. 1,10-Phenanthroline (0.275 g, 1.53 mmol) was added to a solution of the dme adduct **1a** (0.509 g, 1.275 mmol) in 20 mL of THF. After stirring at room temperature for 2 hours the volatiles were removed *in vacuo* resulting in a yellow solid. The material was suspended in 20 mL of diethyl ether and 5 mL of benzene and the resultant was vigorously stirred for 10 minutes. The solids were then collected on a sintered glass frit and were washed with three, 5 mL portions of diethyl ether, followed by three, 2 mL portions of benzene, then three, 2 mL portions of hexane. The resulting pale-yellow powder was then recrystallized from 5 mL of toluene, layered with 5 mL of hexane. The solids were collected and dried *in vacuo* resulting in a pale-yellow powder of analytically pure material. Yield = 0.528 g (1.079 mmol, 85%). X-ray quality crystals were obtained from storing a saturated dichloromethane solution, layered with pentane, at -30 °C for 24 hours. This compound was only sparingly soluble in C<sub>6</sub>D<sub>6</sub>. <sup>1</sup>H NMR (300 MHz, CDCl<sub>3</sub>, ppm): δ 1.70 (s, 18H, C(CH<sub>3</sub>)<sub>3</sub>), 7.84 (dd, 2H, J = 8.1 & 4.8 Hz), 7.92 (s, 2H), 8.44 (d, 2H, J = 8.1 Hz), 9.74 (d, 2H, J = 4.8 Hz). <sup>13</sup>C{<sup>1</sup>H} NMR (75 MHz, CDCl<sub>3</sub>, ppm): δ 30.84 (C(CH<sub>3</sub>)<sub>3</sub>), 72.17 (C(CH<sub>3</sub>)<sub>3</sub>), 124.78, 126.94, 129.78, 138.17, 142.20, 152.55. Selected IR data (KBr, cm<sup>-1</sup>): ν(Mo=N) 1206 (vs), 1246 (s). EA calcd for C<sub>20</sub>H<sub>26</sub>Cl<sub>2</sub>MoN<sub>4</sub> [%]: C, 49.09; H, 5.36; N, 11.45; found [%]: C, 48.98; H, 5.02; N, 11.32.

(*BuN*)<sub>2</sub>MoCl<sub>2</sub>-(*t*BuDAD<sup>H</sup>) **5**. 1,4-Di-*tert*-butyl-1,3-diazabutadiene (0.757 g, 4.498 mmol) was added to a solution of the dme adduct **1a** (1.502 g, 3.762 mmol) in 20 mL of THF. After stirring at room temperature for 2 hours the volatiles were removed *in vacuo* resulting in a yellow solid. The material was suspended in 15 mL of diethyl ether and 10 mL of hexane and the resultant was stirred vigorously for 10 minutes. The solids were then

collected on a sintered glass frit and were washed with three, 2 mL portions of diethyl ether and three, 2 mL portions of hexane. The resulting pale-yellow powder was then recrystallized from 5 mL of toluene, layered with 5 mL of hexane. After 24 hours at  $-30\text{ }^{\circ}\text{C}$  yellow/orange crystals were isolated by decanting the mother-liquor; these were subsequently dried *in vacuo* to yield analytically pure material. The crystals were ground into a fine powder prior to thermal analysis. Yield = 1.445 g (3.027 mmol, 80%).  $^1\text{H}$  NMR (300 MHz,  $\text{C}_6\text{D}_6$ , ppm):  $\delta$  1.45 (s, 18H,  $\text{C}(\text{CH}_3)_3$ ), 1.57 (s, 18H,  $\text{Mo}=\text{NC}(\text{CH}_3)_3$ ), 7.36 (s, 2H,  $\text{N}=\text{CH}$ ).  $^{13}\text{C}\{^1\text{H}\}$  NMR (75 MHz,  $\text{C}_6\text{D}_6$ , ppm):  $\delta$  29.60 ( $\text{C}(\text{CH}_3)_3$ ), 30.93 ( $\text{Mo}=\text{NC}(\text{CH}_3)_3$ ), 62.58 ( $\text{C}(\text{CH}_3)_3$ ), 72.89 ( $\text{Mo}=\text{NC}(\text{CH}_3)_3$ ), 153.06 ( $\text{N}=\text{CH}$ ). Selected IR data (KBr,  $\text{cm}^{-1}$ ):  $\nu(\text{Mo}=\text{N})$  1196 (vs) & 1231 (s);  $\nu(\text{N}=\text{C})$  1454 (m) & 1474 (m). EA calcd for  $\text{C}_{18}\text{H}_{38}\text{Cl}_2\text{MoN}_4$  [%]: C, 45.29; H, 8.02; N, 11.74; found [%]: C, 44.90; H, 7.66; N, 11.33.

$(^t\text{BuN})\text{MoOCl}_2$ - $(^{\text{Bu}}\text{DAD}^{\text{H}})$  **6**. 1,4-Di-*tert*-butyl-1,3-diazabutadiene (0.783 g, 4.653 mmol) was added to a solution of  $(^t\text{BuN})\text{MoOCl}_2$ -dme (1.395 g, 4.054 mmol) in 20 mL of THF. After stirring at room temperature for 2 hours the volatiles were removed *in vacuo* resulting in a green solid. The material was suspended in 5 mL of diethyl ether and 5 mL of pentane and the resultant stirred for 5 minutes. The mixture was then filtered through a sintered glass frit and the solids were washed with three, 3 mL portions of diethyl ether, and three, 3 mL portions of pentane. The solids were collected and dried *in vacuo* resulting in 1.377 g of a greenish-yellow powder. The product was purified by sublimation ( $130\text{ }^{\circ}\text{C}$ , 40 mTorr) onto a water-cooled cold-finger and a yellow powder of analytically pure **6** was obtained. Yield = 1.180 g (2.794 mmol, 69%). X-ray quality crystals were obtained after storing a saturated dichloromethane solution, layered with pentane, at  $-30\text{ }^{\circ}\text{C}$  for 8 hours.  $^1\text{H}$  NMR (300 MHz,  $\text{C}_6\text{D}_6$ , ppm):  $\delta$  1.40 (s, 9H,  $\text{Mo}=\text{NC}(\text{CH}_3)_3$ ), 1.59 & 1.60 (two s, 18 H,  $\text{C}(\text{CH}_3)_3$ ), 6.79 (d, 1H,  $^3J_{\text{HH}} = 1.4\text{ Hz}$ ,  $\text{N}=\text{CH}$ ), 6.88 (d, 1H,  $^3J_{\text{HH}} = 1.4\text{ Hz}$ ,  $\text{N}=\text{CH}$ ).  $^{13}\text{C}\{^1\text{H}\}$  NMR (75 MHz,  $\text{C}_6\text{D}_6$ , ppm):  $\delta$  27.92 ( $\text{C}(\text{CH}_3)_3$ ), 28.48 ( $\text{C}(\text{CH}_3)_3$ ), 29.19 ( $\text{Mo}=\text{NC}(\text{CH}_3)_3$ ), 63.67 ( $\text{C}(\text{CH}_3)_3$ ), 64.47 ( $\text{C}(\text{CH}_3)_3$ ), 74.68 ( $\text{Mo}=\text{NC}(\text{CH}_3)_3$ ), 151.88 ( $\text{N}=\text{CH}$ ), 152.63 ( $\text{N}=\text{CH}$ ). Selected IR data (KBr,  $\text{cm}^{-1}$ ):  $\nu(\text{Mo}=\text{N})$  1201 (s) & 1225 (s);  $\nu(\text{Mo}=\text{O})$  906 (vs);  $\nu(\text{N}=\text{C})$  1454 (m) & 1477 (m). EA calcd for  $\text{C}_{14}\text{H}_{29}\text{Cl}_2\text{MoN}_3\text{O}$  [%]: C, 39.82; H, 6.92; N, 9.95; found [%]: C, 39.53; H, 7.01; N, 9.83.

$(^t\text{BuN})_2\text{MoCl}_2$ - $(^{\text{Pr}}\text{DAD}^{\text{Me}})$  **7**. This compound was prepared following a method analogous to that used to prepare **5** except using 0.750 g (4.457 mmol) of 1,4-di-isopropyl-2,3-dimethyl-1,3-diazabutadiene and 1.502 g (3.762 mmol) of the dme adduct **1a**. Crystallization gave an orange product. Yield = 1.322 g (2.769 mmol, 74%).  $^1\text{H}$  NMR (300 MHz,  $\text{C}_6\text{D}_6$ , ppm):  $\delta$  1.33 (s, 6H,  $\text{N}=\text{C}(\text{CH}_3)_2$ ), 1.50 (d, 12H,  $^3J_{\text{HH}} = 7.0\text{ Hz}$ ,  $\text{CH}(\text{CH}_3)_2$ ), 1.60 (s, 18H,  $\text{C}(\text{CH}_3)_3$ ), 5.03 (br s, 2H,  $\text{CH}(\text{CH}_3)_2$ ).  $^{13}\text{C}\{^1\text{H}\}$  NMR (75 MHz,  $\text{C}_6\text{D}_6$ , ppm):  $\delta$  18.97 (br s,  $\text{N}=\text{C}(\text{CH}_3)_2$ ), 21.36 ( $\text{CH}(\text{CH}_3)_2$ ), 30.79 ( $\text{C}(\text{CH}_3)_3$ ), 56.77 (br s,  $\text{CH}(\text{CH}_3)_2$ ), 71.74 ( $\text{C}(\text{CH}_3)_3$ ), 164.61 ( $\text{N}=\text{C}(\text{CH}_3)_2$ ). Selected IR data (KBr,  $\text{cm}^{-1}$ ):  $\nu(\text{Mo}=\text{N})$  1204 (s) & 1239 (m);  $\nu(\text{N}=\text{C})$  1453 (m) & 1466 (m). EA calcd for  $\text{C}_{18}\text{H}_{38}\text{Cl}_2\text{MoN}_4$  [%]: C, 45.29; H, 8.02; N, 11.74; found [%]: C, 44.93; H, 7.72; N, 11.28.

$(^t\text{BuN})_2\text{MoCl}_2$ - $(^{\text{Cy}}\text{DAD}^{\text{H}})$  **8**. 1,4-Bis(2,6-dimethylphenyl)-1,3-diazabutadiene (0.688 g, 2.603 mmol) was added to a solution of the dme adduct **1a** (1.039 g, 2.603 mmol) in 20 mL of THF. After stirring at room temperature for 2 hours the volatiles were removed *in vacuo* resulting in an orange solid. The material was suspended in 10 mL of pentane and was filtered through a sintered glass frit. The solids were washed with three, 5 mL portions of pentane. The resulting orange solid was then dissolved in a minimal amount of dichloromethane (ca. 3 mL), was layered with 5 mL of pentane, and stored at  $-30\text{ }^{\circ}\text{C}$  for 18 hours resulting in an orange powder. The supernate was carefully removed with a pipette and the powder was washed with five, 2 mL portions of pentane. After drying *in vacuo* the product was isolated as an analytically pure orange powder. Yield = 1.022 g (1.782 mmol, 68%). X-ray quality crystals were obtained after storing a saturated toluene solution, layered with pentane, at  $-30\text{ }^{\circ}\text{C}$  for 24 hours.  $^1\text{H}$  NMR (300 MHz,  $\text{C}_6\text{D}_6$ , ppm):  $\delta$  1.20 (s, 18H,  $\text{C}(\text{CH}_3)_3$ ), 2.63 (s, 12H, *o*- $\text{CH}_3$ ), 6.83 (s, 2H,  $\text{N}=\text{CH}$ ), 6.96 (m, 6H, *m*- $\text{CH}$  & *p*- $\text{CH}$ ).  $^{13}\text{C}\{^1\text{H}\}$  NMR (75 MHz,  $\text{C}_6\text{D}_6$ , ppm):  $\delta$  20.77 (*o*- $\text{CH}_3$ ), 29.64 ( $\text{C}(\text{CH}_3)_3$ ), 71.99 ( $\text{C}(\text{CH}_3)_3$ ),

126.68, 129.00, 130.39, 151.12, 158.94 ( $\text{N}=\text{CH}$ ). Selected IR data (KBr,  $\text{cm}^{-1}$ ):  $\nu(\text{Mo}=\text{N})$  1205 (s) & 1246 (m);  $\nu(\text{N}=\text{C})$  1450 (m) & 1473 (s). EA calcd for  $\text{C}_{26}\text{H}_{38}\text{Cl}_2\text{MoN}_4$  [%]: C, 54.46; H, 6.68; N, 9.77; found [%]: C, 54.46; H, 6.34; N, 9.47.

$(^t\text{BuN})_2\text{MoCl}_2$ -*imp*y **9**. *tert*-Butyl(pyridine-2-yl-methyleneamine) (0.575 g, 3.544 mmol) was added to a solution of the dme adduct **1** (1.311 g, 3.284 mmol) in 20 mL of THF. After stirring at room temperature for 2 hours the volatiles were removed *in vacuo* resulting in an orange solid. Toluene (15 mL) was added to the solid forming a slurry, which was layered with 3 mL of hexane, and the resultant stored at  $-30\text{ }^{\circ}\text{C}$  overnight. The mixture was filtered through a sintered glass frit and the solids were washed with three, 3 mL portions of diethyl ether and three, 3 mL portions of hexane. The solids were collected and dried *in vacuo* resulting in a pale-orange powder of analytically pure material. Yield = 1.263 g (2.680 mmol, 82%). X-ray quality crystals were obtained from storing a saturated 1,2-dimethoxyethane solution, layered with hexane, at  $-30\text{ }^{\circ}\text{C}$  for 48 hours.  $^1\text{H}$  NMR (300 MHz,  $\text{C}_6\text{D}_6$ , ppm):  $\delta$  1.64 (s, 18H,  $\text{Mo}=\text{NC}(\text{CH}_3)_3$ ), 1.69 (s, 9H,  $\text{C}(\text{CH}_3)_3$ ), 6.48 (d, 1H,  $J = 7.6\text{ Hz}$ ), 6.60 (m, 1H), 6.84 (td, 1H,  $J = 7.6$  & 1.7 Hz), 7.68 (s, 1H,  $\text{N}=\text{CH}$ ), 9.37 (d, 1H,  $J = 5.2\text{ Hz}$ ).  $^{13}\text{C}\{^1\text{H}\}$  NMR (75 MHz,  $\text{C}_6\text{D}_6$ , ppm):  $\delta$  29.80 ( $\text{C}(\text{CH}_3)_3$ ), 30.90 ( $\text{Mo}=\text{NC}(\text{CH}_3)_3$ ), 30.99 ( $\text{Mo}=\text{NC}(\text{CH}_3)_3$ ), 63.07 ( $\text{C}(\text{CH}_3)_3$ ), 71.75, ( $\text{Mo}=\text{NC}(\text{CH}_3)_3$ ), 72.46 ( $\text{Mo}=\text{NC}(\text{CH}_3)_3$ ), 125.55, 127.15, 137.87, 149.48, 152.51, 154.12 ( $\text{N}=\text{CH}$ ). Selected IR data (KBr,  $\text{cm}^{-1}$ ):  $\nu(\text{Mo}=\text{N})$  1203 (s), 1241 (m);  $\nu(\text{N}=\text{C})$  1595 (m). EA calcd for  $\text{C}_{18}\text{H}_{32}\text{Cl}_2\text{MoN}_4$  [%]: C, 45.87; H, 6.84; N, 11.89; found [%]: C, 45.52; H, 6.52; N, 11.63.

$(^t\text{BuN})_2\text{MoCl}_2$ -*dm*ampy **10**. 2-(*N,N*-Dimethylamino)methylpyridine (0.236 g, 1.733 mmol) was added to a suspension of the dme adduct **1** (0.600 g, 1.503 mmol) in 15 mL of pentane and 2 mL of toluene. After stirring at room temperature for 18 hours the mixture was filtered through a sintered glass frit giving a yellow solid. The crude product was dissolved in 2 mL of dichloromethane, layered with 2 mL of pentane, and the resultant stored at  $-30\text{ }^{\circ}\text{C}$  for 4 hours giving in yellow, plate-shaped crystals. The mother-liquor was decanted, and the crystals were washed with three, 3 mL portions of pentane. After drying *in vacuo* the product was obtained as a beige-yellow powder. Yield = 0.524 g (1.177 mmol, 78%).  $^1\text{H}$  NMR (300 MHz,  $\text{C}_6\text{D}_6$ , ppm):  $\delta$  1.54 (s, 9H,  $\text{C}(\text{CH}_3)_3$ ), 1.59 (s, 9H,  $\text{C}(\text{CH}_3)_3$ ), 2.55 (s, 6H,  $\text{N}(\text{CH}_3)_2$ ), 3.65 (s, 2H,  $\text{CH}_2$ ), 6.32 (d, 1H,  $J = 7.7\text{ Hz}$ ), 6.62 (m, 1H), 6.83 (td, 1H,  $J = 7.7$  & 1.7 Hz), 9.20 (dd, 1H,  $J = 8.4$  & 0.8 Hz).  $^{13}\text{C}\{^1\text{H}\}$  NMR (75 MHz,  $\text{C}_6\text{D}_6$ , ppm):  $\delta$  30.10 ( $\text{C}(\text{CH}_3)_3$ ), 30.56 ( $\text{C}(\text{CH}_3)_3$ ), 50.35 ( $\text{N}(\text{CH}_3)_2$ ), 65.20 ( $\text{CH}_2$ ), 71.22 ( $\text{C}(\text{CH}_3)_3$ ), 71.87 ( $\text{C}(\text{CH}_3)_3$ ), 122.49, 123.08, 137.99, 153.15, 156.35. Selected IR data (KBr,  $\text{cm}^{-1}$ ):  $\nu(\text{Mo}=\text{N})$  1209 (vs), 1247 (m). EA calcd for  $\text{C}_{16}\text{H}_{30}\text{Cl}_2\text{MoN}_4$  [%]: C, 43.16; H, 6.79; N, 12.58; found [%]: C, 42.96; H, 6.41; N, 12.41.

**Thermal Characterization. Thermogravimetric Analysis.** TGA was performed on a TA Instruments Q500 instrument which was housed in a "chemical-free", nitrogen-filled (99.998%) MBraun Labmaster 130 glovebox. In a typical experiment  $10.000 \pm 0.100$  mg of analyte was placed in a platinum pan and was heated to  $500\text{ }^{\circ}\text{C}$  with a ramp rate of  $10\text{ }^{\circ}\text{C min}^{-1}$ , unless otherwise stated, using nitrogen (99.999% purity, 60 sccm) as the purge gas. Platinum pans were cleaned by sequential sonication in glacial acetic acid then isopropanol, followed by heating until red-hot with a propane torch. Langmuir vapor pressure equations were derived from TGA data using a previously reported method, employing benzoic acid as the calibrant.<sup>[55,56]</sup>

**Differential Scanning Calorimetry.** DSC experiments were performed with a TA Instruments Q10 instrument. The DSC was calibrated at the melting point of indium metal ( $156.6\text{ }^{\circ}\text{C}$ ). All DSC samples were hermetically sealed in aluminium pans inside a glovebox prior to analysis. Due to the volatile nature of the analytes and their decomposition products, mass loadings greater than 1 mg often ruptured the sealed pans. Therefore, small mass loadings of  $<1$  mg were typically used for all DSC experiments. Unless otherwise stated, all samples were heated to  $400\text{ }^{\circ}\text{C}$  with a ramp rate of  $10\text{ }^{\circ}\text{C min}^{-1}$ , using nitrogen (99.998% purity) as the purge gas.

**X-Ray Crystallography.** Deposition Numbers 2123336 (**2b**), 2123333 (**2c**), 2123332 (**2d**), 2123334 (**3a**), 2123327 (**3a-C<sub>7</sub>H<sub>8</sub>**), 2123325 (**3b**), 2123331 (**3c**), 2123335 (**4**), 2123329 (**5**), 2123328 (**6**), 2123330 (**7**), 2123326 (**8**), 2123323 (**9**), 2123318 (**10**), 2123321 (MoO<sub>2</sub>Cl<sub>2</sub>-dme), 2123319 (*bis-N,N'*-(2-chloroacetyl)-2,5-dimethylhexane-2,5-diamine), 2123322 ([*imtpaH*][(<sup>t</sup>BuN)<sub>2</sub>MoCl<sub>3</sub>]), 2123320 ((<sup>t</sup>BuN)<sub>2</sub>MoCl<sub>2</sub>-(4,4'-dimethyl-2,2'-dipyridyl)), and 2123324 ((<sup>t</sup>BuN)<sub>2</sub>MoCl<sub>2</sub>-(<sup>o</sup>PeDAD<sup>H</sup>)) contain the supplementary crystallographic data for this paper. These data are provided free of charge by The Cambridge Crystallographic Data Centre. The crystallographic diagrams were prepared using ORTEP-3 for Windows.<sup>[76]</sup> Specific details about data collection and refinements can be found in the Supporting Information.

## Acknowledgements

M.A.L. thanks the Natural Sciences and Engineering Council of Canada (NSERC) for funding through the Alexander Graham Bell CGS-D Scholarship. S.T.B. acknowledges NSERC for support through the Discovery Grants Program (RGPIN-2019-06213). Finally, we also thank Sharon Curtis and Peter Pallister, from the University of Ottawa, for HRMS and LT-NMR acquisition, and Lara Watanabe, from the University of Windsor, for EA acquisition.

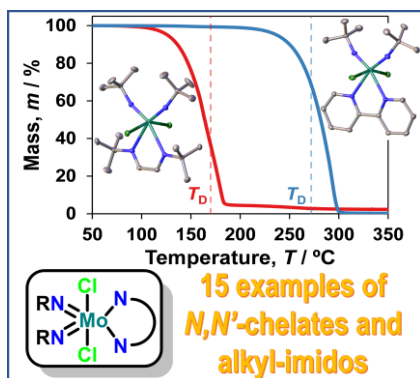
**Keywords:** Thermal Stability • Volatility • Precursor Design • Molybdenum • Thermogravimetric Analysis • Chemical Structure

[1] Y. He, J. Y. Feng, *J. Cryst. Growth* **2004**, *263*, 203–207.  
 [2] M. Führer, T. Van Haasterecht, J. H. Bitter, *Catal. Sci. Technol.* **2020**, *10*, 6089–6097.  
 [3] M. Mattinen, J.-L. Wree, N. Stegmann, E. Ciftiyurek, M. El Achhab, P. J. King, K. Mizohata, J. Räisänen, K. D. Schierbaum, A. Devi, M. Ritala, M. Leskelä, *Chem. Mater.* **2018**, *30*, 8690–8701.  
 [4] A. Splendiani, L. Sun, Y. Zhang, T. Li, J. Kim, C. Y. Chim, G. Galli, F. Wang, *Nano Lett.* **2010**, *10*, 1271–1275.  
 [5] T. Spalvins, *J. Vac. Sci. Technol. A Vacuum, Surfaces, Film.* **1987**, *5*, 212–219.  
 [6] V. Miikkulainen, M. Leskelä, M. Ritala, R. L. Puurunen, *J. Appl. Phys.* **2013**, *113*, 021301.  
 [7] S. T. Barry, *Chemistry of Atomic Layer Deposition*, De Gruyter, Berlin, Boston, **2021**.  
 [8] S. T. Barry, *Coord. Chem. Rev.* **2013**, *257*, 3192–3201.  
 [9] K. Bernal Ramos, M. J. Saly, Y. J. Chabal, *Coord. Chem. Rev.* **2013**, *257*, 3271–3281.  
 [10] O. M. El-Kadri, M. J. Heeg, C. H. Winter, *J. Chem. Soc. Dalton Trans.* **2006**, 1943–1953.  
 [11] V. Miikkulainen, M. Suvanto, T. A. Pakkanen, *Chem. Mater.* **2007**, *19*, 263–269.  
 [12] V. Miikkulainen, M. Suvanto, T. A. Pakkanen, *Chem. Vap. Depos.* **2008**, *14*, 71–77.  
 [13] A. Bertuch, G. Sundaram, M. Saly, D. Moser, R. Kanjolia, *J. Vac. Sci. Technol. A Vacuum, Surfaces, Film.* **2014**, *32*, 01A119.  
 [14] M. F. J. Vos, B. Maccio, N. F. W. Thissen, A. A. Bol, W. M. M. (Erwin) Kessels, *J. Vac. Sci. Technol. A Vacuum, Surfaces, Film.* **2016**, *34*, 01A103.  
 [15] A. Sharma, M. A. Verheijen, L. Wu, S. Karwal, V. Vandalon, H. C. M. Knoops, R. S. Sundaram, J. P. Hofmann, W. M. M. Kessels, A. A. Bol, *Nanoscale* **2018**, *10*, 8615–8627.  
 [16] H. Sopha, A. T. Tesfaye, R. Zazpe, J. Michalicka, F. Dvorak, L. Hromadko, M. Krbal, J. Prikryl, T. Djenizian, J. M. Macak, *FlatChem*

**2019**, *17*, 100130.  
 [17] B. Kalanyan, R. Beams, M. B. Katz, A. V. Davydov, J. E. Maslar, R. K. Kanjolia, *J. Vac. Sci. Technol. A* **2019**, *37*, 010901.  
 [18] A. Bertuch, B. D. Keller, N. Ferralis, J. C. Grossman, G. Sundaram, *J. Vac. Sci. Technol. A Vacuum, Surfaces, Film.* **2017**, *35*, 01B141.  
 [19] Y. K. Cho, Y. Choi, S.-G. Kim, Y. Jun, H. Kim, *Thin Solid Films* **2019**, *692*, 137607.  
 [20] M. I. Chowdhury, M. Sowa, A. C. Kozen, B. A. Krick, J. Haik, T. F. Babuska, N. C. Strandwitz, *J. Vac. Sci. Technol. A* **2021**, *39*, 012407.  
 [21] V. Vandalon, A. A. Bol, M. A. Verheijen, W. M. M. Kessels, *ACS Appl. Nano Mater.* **2020**, *3*, 10200–10208.  
 [22] V. Gwildies, T. B. Thiede, S. Amirjalayer, L. Alsamman, A. Devi, R. A. Fischer, *Inorg. Chem.* **2010**, *49*, 8487–8494.  
 [23] T. Thiede, V. Gwildies, L. Alsamann, D. Rische, R. Fischer, in *ECS Trans.*, ECS, **2009**, pp. 593–600.  
 [24] J. L. Wree, E. Ciftiyurek, D. Zanders, N. Boysen, A. Kostka, D. Rogalla, M. Kasischke, A. Ostendorf, K. Schierbaum, A. Devi, *Dalton Trans.* **2020**, *49*, 13462–13474.  
 [25] S. Cwik, D. Mitoraj, O. Mendoza Reyes, D. Rogalla, D. Peeters, J. Kim, H. M. Schütz, C. Bock, R. Beranek, A. Devi, *Adv. Mater. Interfaces* **2018**, *5*, 1–11.  
 [26] N. B. Srinivasan, T. B. Thiede, T. de los Arcos, V. Gwildies, M. Krasnopolski, H. W. Becker, D. Rogalla, A. Devi, R. A. Fischer, *Surf. Coatings Technol.* **2013**, *230*, 130–136.  
 [27] C. L. Dezelah IV, O. M. El-Kadri, M. J. Heeg, C. H. Winter, *J. Mater. Chem.* **2004**, *14*, 3167–3176.  
 [28] D. Rische, MOCVD of Tungsten and Molybdenum Nitrides, Ph.D. Thesis, University of Bochum, Bochum, Germany, 2007.  
 [29] Y. Jang, J. B. Kim, T. E. Hong, S. J. Yeo, S. Lee, E. A. Jung, B. K. Park, T. M. Chung, C. G. Kim, D. J. Lee, H. B. R. Lee, S. H. Kim, *J. Alloys Compd.* **2016**, *663*, 651–658.  
 [30] N. C. Ou, K. Preradovic, E. T. Ferenczy, C. B. Sparrow, I. M. Germaine, T. Jurca, V. Craciun, L. Mcelwee-White, *Organometallics* **2020**, *39*, 956–966.  
 [31] H. T. Chiu, W. Y. Ho, S. H. Chuang, *J. Mater. Res.* **1994**, *9*, 1622–1624.  
 [32] H.-T. Chiu, G.-B. Chang, W.-Y. Ho, S.-H. Chuang, G.-H. Lee, S.-M. Peng, *J. Chinese Chem. Soc.* **1994**, *41*, 755–761.  
 [33] M. A. Land, K. N. Robertson, S. T. Barry, *Organometallics* **2020**, *39*, 916–927.  
 [34] H. H. Fox, K. B. Yap, J. Robbins, S. Cai, R. R. Schrock, *Inorg. Chem.* **1992**, *31*, 2287–2289.  
 [35] P. W. Dyer, V. C. Gibson, J. A. K. Howard, B. Whittle, C. Wilson, *J. Chem. Soc., Chem. Commun.* **1992**, *04*, 1666–1668.  
 [36] E. N. Nikolaevskaya, N. O. Druzhkov, M. A. Syroeshkin, M. P. Egorov, *Coord. Chem. Rev.* **2020**, *417*, 213353.  
 [37] A. Merkoulou, 1,4-Diazadiene Imido Complexes of Group V and VI Elements and Their Application in Chemical Vapour Deposition of TaN Films. Ph.D. Thesis, Philipps University of Marburg, Marburg, Germany, 2005.  
 [38] F. E. Kühn, A. D. Lopes, A. M. Santos, E. Herdtweck, J. J. Haider, C. C. Romão, A. G. Santos, *J. Mol. Catal. A Chem.* **2000**, *151*, 147–160.  
 [39] T. Pugh, S. D. Cosham, J. A. Hamilton, A. J. Kingsley, A. L. Johnson, *Inorg. Chem.* **2013**, *52*, 13719–13729.  
 [40] T. J. Knisley, M. J. Saly, M. J. Heeg, J. L. Roberts, C. H. Winter, *Organometallics* **2011**, *30*, 5010–5017.  
 [41] L. D. Jason, D. M. Caleb, J. S. Michael, D. J. Nathan, P. J. Ragogna,

- Inorg. Chem.* **2009**, *48*, 3239–3247.
- [42] M. W. Day, A. Wong-Foy, J. E. Bercaw, CCDC 101107: CSD Communication, 2003.
- [43] N. D. Schley, G. E. Dobereiner, R. H. Crabtree, *Organometallics* **2011**, *30*, 4174–4179.
- [44] A. Bruneau-Voisine, D. Wang, V. Dorcet, T. Roisnel, C. Darcel, J. B. Sortais, *Org. Lett.* **2017**, *19*, 3656–3659.
- [45] F. Z. Yang, Y. H. Wang, M. C. Chang, K. H. Yu, S. L. Huang, Y. H. Liu, Y. Waang, S. T. Liu, J. T. Chen, *Inorg. Chem.* **2009**, *48*, 7639–7644.
- [46] J. B. Alexander, R. R. Schrock, W. M. Davis, K. C. Hultsch, A. H. Hoveyda, J. H. Houser, *Organometallics* **2000**, *19*, 3700–3715.
- [47] Our attempts to prepare (PrN)<sub>2</sub>MoCl<sub>2</sub> consistently led to an intractable black residue and the only similar known compound is (PrN)(DippN)WCl<sub>2</sub>-dme (Dipp = 2,6-diisopropylphenyl); A. M. Messinis, A. S. Batsanov, W. R. H. Wright, J. A. K. Howard, M. J. Hanton, P. W. Dyer, *ACS Catal.* **2018**, *8*, 11249–11263.
- [48] D. C. Rosenfeld, P. T. Wolczanski, K. A. Barakat, C. Buda, T. R. Cundari, F. C. Schroeder, E. B. Lobkovsky, *Inorg. Chem.* **2007**, *46*, 9715–9735.
- [49] U. Siemeling, L. Kölling, O. Kuhnert, B. Neumann, A. Stammeler, H. G. Stammeler, G. Fink, E. Kaminski, A. Kiefer, R. R. Schrock, *Zeitschrift für Anorg. und Allg. Chemie* **2003**, *629*, 781–792.
- [50] P. W. Dyer, V. C. Gibson, J. A. K. Howard, B. Whittle, C. Wilson, *Polyhedron* **1995**, *14*, 103–111.
- [51] D. Grant, M. A. McKervey, J. J. Rooney, N. G. Samman, G. Step, *J. Chem. Soc., Chem. Commun.* **1972**, 1186.
- [52] G. L. Buchanan, *Chem. Soc. Rev.* **1974**, *3*, 41.
- [53] P. Barrie, T. A. Coffey, G. D. Forster, G. Hogarth, *J. Chem. Soc. Dalton Trans.* **1999**, 4519–4528.
- [54] K. Dreisch, C. Andersson, C. Stålhandske, *Polyhedron* **1993**, *12*, 1335–1343.
- [55] D. M. Price, *Thermochim. Acta* **2001**, *367–368*, 253–262.
- [56] D. M. Price, *Thermochim. Acta* **2015**, *622*, 44–50.
- [57] J. P. Coyle, A. Kurek, P. J. Pallister, E. R. Sirianni, G. P. A. Yap, S. T. Barry, *Chem. Commun.* **2012**, *48*, 10440.
- [58] M. B. E. Griffiths, Z. S. Dubrawski, G. Bačić, A. Japahuge, J. D. Masuda, T. Zeng, S. T. Barry, *Eur. J. Inorg. Chem.* **2019**, *2019*, 4927–4938.
- [59] J. E. Bol, B. Hessen, J. H. Teuben, W. J. J. Smeets, A. L. Spek, *Organometallics* **1992**, *11*, 1981–1983.
- [60] F. Muller, G. Van Koten, M. J. A. Kraakman, K. Vrieze, R. Zoet, K. A. A. Duineveld, D. Heijdenrijk, C. H. Stam, M. C. Zoutberg, *Organometallics* **1989**, *8*, 982–991.
- [61] F. Muller, G. van Koten, K. Vrieze, K. A. A. Duineveld, D. Heijdenrijk, A. N. S. Mak, C. H. Stam, *Organometallics* **1989**, *8*, 1324–1330.
- [62] G. K. Cantrell, T. Y. Meyer, *Organometallics* **1997**, *16*, 5381–5383.
- [63] G. K. Cantrell, T. Y. Meyer, *Chem. Commun.* **1997**, 1551–1552.
- [64] G. K. Cantrell, T. Y. Meyer, *J. Am. Chem. Soc.* **1998**, *120*, 8035–8042.
- [65] S. E. Koponen, P. G. Gordon, S. T. Barry, *Polyhedron* **2016**, *108*, 59–66.
- [66] D. A. Edwards, G. W. A. Fowles, *J. Less-Common Met.* **1961**, *3*, 181–187.
- [67] S. B. Kim, P. Sinsermsuksakul, A. S. Hock, R. D. Pike, R. G. Gordon, *Chem. Mater.* **2014**, *26*, 3065–3073.
- [68] N. De Kimpe, L. D'Hondt, E. Stanoeva, *Tetrahedron Lett.* **1991**, *32*, 3879–3882.
- [69] J. S. Kingsbury, A. H. Hoveyda, *J. Am. Chem. Soc.* **2005**, *127*, 4510–4517.
- [70] B. A. Riga, Y. F. Silva, O. R. Nascimento, A. E. H. Machado, V. P. Carvalho-Jr, B. E. Goi, *Polyhedron* **2020**, *192*, 114870.
- [71] D. C. Rogness, N. A. Markina, J. P. Waldo, R. C. Larock, *J. Org. Chem.* **2012**, *77*, 2743–2755.
- [72] M. Irfan, L. Ge, Y. Wang, Z. Yang, T. Xu, *ACS Sustain. Chem. Eng.* **2019**, *7*, 4429–4442.
- [73] N. L. Hill, R. Braslau, *Macromolecules* **2005**, *38*, 9066–9074.
- [74] K. A. Rufanov, D. N. Zarubin, N. A. Ustynyuk, D. N. Gourevitch, J. Sundermeyer, A. V. Churakov, J. A. K. Howard, *Polyhedron* **2001**, *20*, 379–385.
- [75] R. Ramnauth, S. Al-Juaid, M. Motevalli, B. C. Parkin, A. C. Sullivan, *Inorg. Chem.* **2004**, *43*, 4072–4079.
- [76] L. J. Farrugia, *J. Appl. Crystallogr.* **2012**, *45*, 849–854.

## Entry for the Table of Contents



A series of *bis*(alkylimido)-dichloromolybdenum(VI) compounds, which include different neutral  $N,N'$ -chelating ligands, as well as different alkyl imido groups, were prepared and characterized. The effect each component had on volatility and thermal stability was investigated and compared. Several compounds that exhibit excellent volatility and thermal stability have been identified. Finally, most compounds followed the same primary decomposition pathway,  $\gamma$ -H activation.

Institute and/or researcher Twitter usernames: @MikeL4nd, @sean\_t\_barry, @Carletonchem, @SMUCHEMISTRY